AIP | Physics of Fluids

Swimming and pumping by helical waves in viscous and viscoelastic fluids

Lei Li and Saverio E. Spagnolie

Citation: Physics of Fluids (1994-present) **27**, 021902 (2015); doi: 10.1063/1.4909516
View online: http://dx.doi.org/10.1063/1.4909516
View Table of Contents: http://scitation.aip.org/content/aip/journal/pof2/27/2?ver=pdfcov
Published by the AIP Publishing

PHYSICS OF FLUIDS **27**, 021902 (2015)

Swimming and pumping by helical waves in viscous and viscoelastic fluids

Lei Li[a)] and Saverio E. Spagnolie[b)]
Department of Mathematics, University of Wisconsin-Madison, 480 Lincoln Dr., Madison, Wisconsin 53706, USA

(Received 16 August 2014; accepted 8 January 2015; published online 26 February 2015)

We study helical bodies of arbitrary cross-sectional profile as they swim or transport fluid by the passage of helical waves. Many cases are explored: the external flow problem of swimming in a cylindrical tube or an infinite domain, the internal fluid pumping problem, and confined/unconfined swimming and internal pumping in a viscoelastic (Oldroyd-B) fluid. A helical coordinate system allows for the analytical calculation of swimming and pumping speeds and fluid velocities in the asymptotic regime of nearly cylindrical bodies. In a Newtonian flow, a matched asymptotic analysis results in corrections to the swimming speed accurate to fourth-order in the small wave amplitude, and the results compare favorably with full numerical simulations. We find that the torque-balancing rigid body rotation generally opposes the direction of wave passage, but not always. Confinement can result in local maxima and minima of the swimming speed in the helical pitch, and the effects of confinement decrease exponentially fast with the diameter of the tube. In a viscoelastic fluid, we find that the effects of fluid elasticity on swimming and internal pumping modify the Newtonian results through the mode-dependent complex viscosity, even in a confined domain. © *2015 AIP Publishing LLC.* [http://dx.doi.org/10.1063/1.4909516]

I. INTRODUCTION

The fluid mechanics of swimming in viscous environments is a central problem in many biological and engineering processes.[1] A common mechanism of propulsion at the micro-scale is the passage of waves atop the surface of a cell body, either by surface deformations or by metachronal ciliary activity (see Figs. 1(a)-1(b)).[2–4] The ciliary waves of numerous organisms, including *Paramecia*, *Opalina*, and *Volvox*, are helically arranged, so that the organisms rotate as they swim;[3,5] *Volvox* is named for its spinning motion (from the Latin *volvere*, to roll).[6] Helical and inhomogeneous arrangements of cilia can also lead to helical swimming trajectories in free space[3,7] and in confined domains,[8–10] and the double-helical structure of some insect spermatozoa can result in double-helical swimming trajectories.[11] Meanwhile, the motility mechanism of the marine cyanobacterium *Synechococcus* is still an open problem in biophysics.[12–15] *Synechococcus* is known to swim absent the presence of a substrate, without changing shape, and without any observable external organelles (see Fig. 1(c)). However, it has recently been argued that a continuous looped helical track like that found in the gliding organism *Myxococcus xanthus* may also be present in *Synechococcus* (see Fig. 1(d)), which suggests the possibility of helical wave locomotion, an argument that is strengthened by an observed body rotation during swimming.[16]

Theoretical models of microorganisms swimming by surface distortions extend back to the work of Taylor,[20] Lighthill,[21] Blake,[3,22,23] and Brennen[24] (see also the text by Childress[25]). For the study of ciliary locomotion in these works, "envelope" models were developed in which the tips of the cilia are assumed to form a continuous and undulating boundary. Stone and Samuel used the

a)leili@math.wisc.edu
b)spagnolie@math.wisc.edu

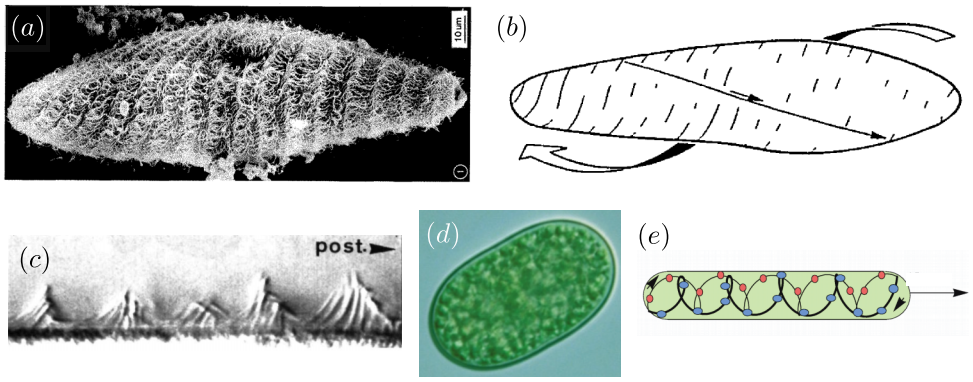

FIG. 1. (a) A scanning electron micrograph of the ciliated *Paramecium*, with a clear helical structure (Reprinted with permission from Tamm, "Ciliary motion in paramecium a scanning electron microscope study," J. Cell Biol. **55**, 250–255 (1972). Copyright 1972 Rockefeller University Press.[17]). (b) Wave fronts indicate patterns of ciliary beating based on quantified data of wavelengths and wave angle. Small arrow: beat direction; long arrow: direction of metachronal waves; helical arrow: swimming direction and rotation (Reprinted with permission from Machemer, "Ciliary activity and the origin of metachrony in Paramecium: Effects of increased viscosity," J. Exp. Biol. **57**, 239–259 (1972). Copyright, 1972 Company of Biologists Ltd.). (c) Metachronal wave profile of *Paramecium* (dorsal surface). The approximation of the amplitude of the ciliary envelope may be best approximated as smaller than half the cilium length[18] (Reprinted with permission from Machemer, "Ciliary activity and the origin of metachrony in Paramecium: Effects of increased viscosity," J. Exp. Biol. **57**, 239–259 (1972). Copyright, 1972 Company of Biologists Ltd.). (d) The propulsive mechanism of the cyanobacterium *Synechococcus* is a biophysical mystery. (Reprinted with permission from Y. Tsukii, Protist Information Server, 2005, url: http://protist.i.hosei.ac.jp/.)[82] (e) It has been proposed that *Synechococcus* swims by small amplitude surface deformations generated by cargo-carrying protein motors moving along a continuous looped helical track near the cell membrane.[19]

Lorentz reciprocal identity to determine the swimming speed of such a body by an integration over the surface distortion velocity and the surface stress in a related resistance problem.[14] These classical considerations have been extended recently to the study of many-swimmer interactions (e.g., the "dancing" of *Volvox*),[5,26,27] wall-interactions,[28–31] generalized squirming motion,[32] the stirring of fluid,[33] unsteady swimming,[34] swimming in complex fluids,[35–37] optimal swimming strokes,[38–40] the emergence of metachronal waves,[41] confined swimming,[42] and submerged robotics.[43] The propulsion of infinitely long bodies by helical waves has been explored analytically by Chwang and Wu,[44] Higdon,[45] and Felderhof,[46] numerically by Higdon,[47] Phan-Thien *et al.*[48] and Liu *et al.*[49,65] and in viscoelastic flows by Fu *et al.*[50] and Spagnolie *et al.*[51]

Meanwhile, the flow internal to a near-cylinder generated by surface undulations may have applications in the mucociliary clearance of the lungs.[3,52–56] Many other cilia-driven internal flows have been studied; for instance, an envelope model was applied in the study of ciliary transport in the male reproductive tract,[57] which was unsuccessful in matching experimental results, likely because cilia in tubules undergo antiplectic as opposed to symplectic metachronal waves. In the former, the apparent envelope defined by the tips of the cilia passes in waves in the direction of the recovery stroke of the cilia, while in the latter, the waves pass in the direction of the power stroke.[3] Other models that treat each cilium separately are more accurate in this setting.[58]

In a previous paper, we solved the Stokes equations of viscous flow in a helical coordinate system to study the locomotion of helical bodies of arbitrary cross-sectional geometry undergoing rigid body translation and rotation.[59] Analytical expressions for the force-free swimming speed and torque were derived in the asymptotic regime of nearly cylindrical bodies. In this paper, we investigate instead the swimming of an infinitely long body by the passage of helical waves along its surface. Many cases are explored: the external flow problem for force- and torque-free swimming in a cylindrical tube or an infinite domain, the internal fluid pumping problem, and confined/unconfined swimming and internal pumping in a viscoelastic (Oldroyd-B) fluid. The swimming and pumping speeds and fluid velocities are derived in the asymptotic regime of nearly cylindrical bodies. Closed form analytical solutions are developed up to second order in the small wave amplitude. In a Newtonian flow, a matched asymptotic analysis yields corrections to the analytical expressions at fourth

order in the wave amplitude in the swimming problem, and the predicted swimming speeds and pumping rates are compared to numerical solutions of the full Stokes equations.

The asymptotic matching of the flow in the small region near the body where the flow is varying rapidly to a smooth external flow is reminiscent of the "oscillating boundary layer" model of swimming explored by Brennen.[24] A similar boundary layer that develops for small helical pitch in the external swimming problem is also observed in the internal pumping problem, and the internal flow exhibits helical structures that recede towards the boundary in this limit. For swimming inside a cylindrical tube, we find that the swimming speed can develop local maxima and minima in the helical pitch, and that the effects of confinement decrease exponentially fast with the tube diameter. Finally, we show how swimming and pumping in a viscoelastic fluid are modified by a mathematically simple form via the mode-dependent complex viscosity, even for swimming in a confined domain.

The paper is organized as follows. The equations of motion, helical coordinate system, and numerical method are introduced in Sec. II. In Sec. III, the external flow problem is considered, where we find the swimming speed and rotation rate of a helical body in a cylindrical tube or an infinite domain. In Sec. IV, we turn our attention to the internal flow problem, where the flow structure and rate of fluid transport are determined. The leading order swimming speed and pumping rates for helical wave motion in a viscoelastic (Oldroyd-B) fluid are presented in Sec. V. We conclude with a brief discussion in Sec. VI.

II. SETUP

A. Body geometry, equations of motion, and helical coordinate system

In the exploration to follow, we will consider a helical wave superimposed onto a cylinder of radius A and infinite length aligned with the $\hat{\mathbf{z}}$ axis, confined by a cylindrical tube of radius L^*. The surface at time $t = 0$ is described by

$$\mathbf{x}^S(\theta,\zeta) = A\rho(\theta)\,[\cos(\nu^*\zeta+\theta)\hat{\mathbf{x}} + \sin(\nu^*\zeta+\theta)\hat{\mathbf{y}}] + \zeta\hat{\mathbf{z}}, \tag{1}$$

where $\theta \in [0,2\pi)$ and $\zeta \in (-\infty,\infty)$, and $2\pi/\nu^*$ is the helical pitch (the pitch angle of the helical wave is given by $\beta = \tan^{-1}(\nu^* A)$). The dimensionless function $\rho(\theta)$ describes the cross-sectional profile. Examples of instantaneous body shapes with different profiles are shown in Figs. 2(a)-2(c), and motion inside a cylindrical tube is shown in Fig. 2(d). Assuming that helical waves pass over the base cylinder with frequency ω, the surface is usefully written in terms of a material coordinate $\varphi = \theta + \nu^*\zeta + \omega t$ which is invariant for a material point,

$$\mathbf{x}^S(\varphi,\zeta,t) = A\,\rho(\varphi-\nu^*\zeta-\omega t)\,[\cos(\varphi+\Omega^* t)\,\hat{\mathbf{x}} + \sin(\varphi+\Omega^* t)\,\hat{\mathbf{y}}] + (\zeta + U^* t)\,\hat{\mathbf{z}}, \tag{2}$$

where U^* is the swimming speed and Ω^* is a counterbalancing rigid body rotation which is generally non-zero if the body is torque-free. The material on the helical surface then moves with velocity $\mathbf{u}^S(\varphi,\zeta,t) = \partial\mathbf{x}^S(\varphi,\zeta,t)/\partial t$. Anticipating the study of nearly cylindrical bodies, we write $\rho(\theta) = 1 + \varepsilon f(\theta)$, where $\varepsilon \ll 1$ and $f(\theta)$ is a 2π-periodic function; then at $t = 0$, the surface velocity may be written as

$$\begin{aligned}\mathbf{u}^S(\theta,\zeta) = {}& -\varepsilon\omega\, A f'(\theta)\,[\cos(\nu^*\zeta+\theta)\,\hat{\mathbf{x}} + \sin(\nu^*\zeta+\theta)\,\hat{\mathbf{y}}] \\ & + \Omega^* A\rho(\theta)\,[-\sin(\nu^*\zeta+\theta)\,\hat{\mathbf{x}} + \cos(\nu^*\zeta+\theta)\,\hat{\mathbf{y}}] + U^*\hat{\mathbf{z}}.\end{aligned} \tag{3}$$

The equations of momentum and mass conservation in an incompressible flow in the viscous (zero Reynolds number) limit are given by

$$\nabla\cdot\boldsymbol{\sigma} = -\nabla p + \nabla\cdot\boldsymbol{\tau} = \mathbf{0}, \quad \nabla\cdot\mathbf{u} = 0, \tag{4}$$

where $\boldsymbol{\sigma} = -p\mathbf{I} + \boldsymbol{\tau}$ is the fluid stress, with p the pressure, $\boldsymbol{\tau}$ is the deviatoric stress, and $\mathbf{u}$ is the fluid velocity. In a Newtonian fluid, the stress is linear in the symmetric rate-of-strain, $\boldsymbol{\tau} = \mu(\nabla\mathbf{u} + \nabla\mathbf{u}^T)$, where μ is the viscosity, and the momentum balance equation in Eq. (4) takes the form $-\nabla p + \mu\nabla^2\mathbf{u} = \mathbf{0}$. The system is made dimensionless by scaling lengths on A, time on $1/\omega$, velocities on $A\,\omega$, and

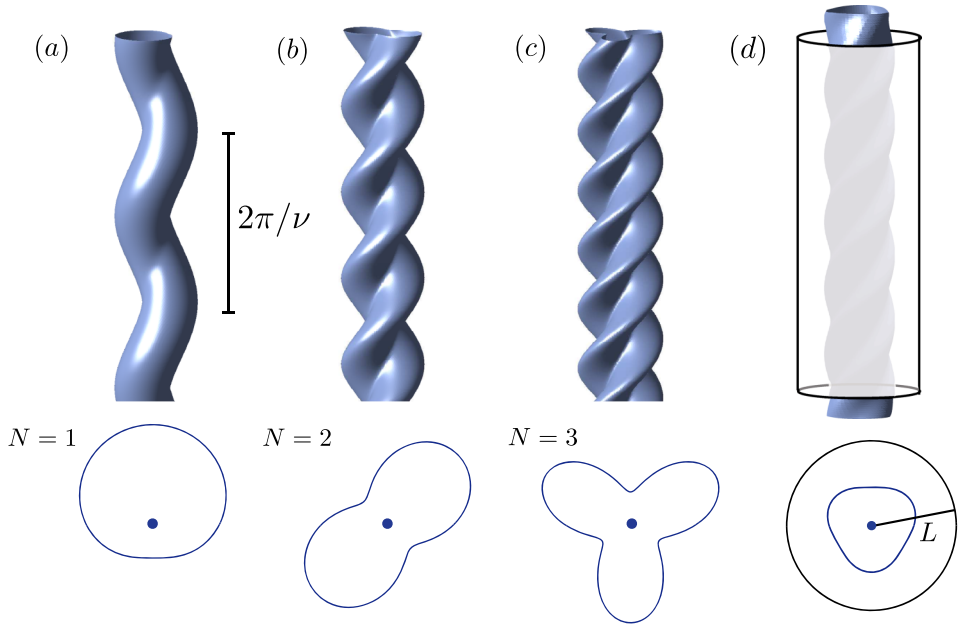

FIG. 2. Examples of helical bodies with $\nu = 1$ (the helical pitch is $2\pi/\nu$), and cross section parameterizations given by (a) $\rho(\theta) = 1 + (1/2)\sin(\theta)$; (b) $\rho(\theta) = 1 + (1/2)\sin(2\theta)$; (c) $\rho(\theta) = 1 + (1/2)\sin(3\theta)$. Cross sections in the $z = 0$ plane are also shown. (d) A helical swimmer with $\rho(\theta) = 1 + (1/10)\sin(3\theta)$ inside a cylindrical tube of radius $L = 2$.

stresses on $\mu\omega$. The dimensionless swimming speed and rigid body rotation rate are written as $U = U^*/(A\omega)$ and $\Omega = \Omega^*/\omega$, the cylindrical tube has dimensionless radius $L = L^*/A$, and we define $\nu = \nu^* A$. All variables are henceforth understood to be dimensionless unless otherwise stated. Since time does not appear in the Stokes equations, the flow is solved without loss of generality at $t = 0$ and we omit the t dependence for notational convenience.

Application of the same non-dimensionalization to Newton's second law reveals that the body is force- and torque-free in the zero Reynolds number limit. For neutrally buoyant organisms, the swimming must therefore be free of a net hydrodynamic force or torque. A consequence of the torque-free condition, for example, is that organisms such as *Paramecium* and *Volvox* for which metachronal ciliary waves pass along the surface at an angle must also rotate as a rigid body to balance the torque, generally in the opposite direction as the wave passage, as we will show.

In this work, we will make use of a helical coordinate system, (r, θ, ζ), denoting a point in space $\mathbf{x}$ by

$$\mathbf{x} = r\,[\cos(\nu\zeta + \theta)\hat{\mathbf{x}} + \sin(\nu\zeta + \theta)\hat{\mathbf{y}}] + \zeta\,\hat{\mathbf{z}}, \tag{5}$$

along with orthonormal basis vectors, $(\hat{\mathbf{r}}, \hat{\boldsymbol{\theta}}, \hat{\mathbf{z}})$, where

$$\hat{\mathbf{r}} = \cos(\nu\zeta + \theta)\hat{\mathbf{x}} + \sin(\nu\zeta + \theta)\hat{\mathbf{y}},\ \hat{\boldsymbol{\theta}} = -\sin(\nu\zeta + \theta)\hat{\mathbf{x}} + \cos(\nu\zeta + \theta)\hat{\mathbf{y}}. \tag{6}$$

The gradient operator in this coordinate system is given by

$$\nabla = \hat{\mathbf{r}}\,\frac{\partial}{\partial r} + \hat{\boldsymbol{\theta}}\frac{1}{r}\frac{\partial}{\partial\theta} + \hat{\mathbf{z}}\left(\frac{\partial}{\partial\zeta} - \nu\frac{\partial}{\partial\theta}\right). \tag{7}$$

Leaning on the helical symmetry of the problem, in every case considered in the paper, we will consider solutions of the form

$$\mathbf{u}(r,\theta,\zeta) = u(r,\theta)\hat{\mathbf{r}} + v(r,\theta)\hat{\boldsymbol{\theta}} + w(r,\theta)\hat{\mathbf{z}}, \quad p(r,\theta,\zeta) = p(r,\theta). \tag{8}$$

B. Numerical method

The helical symmetry of the problem is of great use in developing a fast and high-order accurate numerical method. Our numerical approach is based on the second kind boundary integral formulation of the Stokes equations.[60,61] In this formulation, the dimensionless fluid velocity at a point $\mathbf{x}$ in the fluid between a helical body and a cylindrical container (in the lab frame) is represented as an integration over the immersed boundary ∂S and the container boundary ∂S_C,

$$\mathbf{u}_{lab}(\mathbf{x}) = \int_{\partial S} \mathbf{q}(\mathbf{y}) \cdot \mathbf{T}(\mathbf{x},\mathbf{y}) \cdot \hat{\mathbf{n}}(\mathbf{y})\, dS_y + \int_{\partial S_C} \mathbf{h}(\mathbf{y}) \cdot \mathbf{T}(\mathbf{x},\mathbf{y}) \cdot \hat{\mathbf{n}}(\mathbf{y})\, dS_y. \tag{9}$$

Here, the integration variable $\mathbf{y}$ describes either the surface from Eq. (1) or the surface of the cylindrical tube, dS_y is the surface area element, $T_{ijk}(\mathbf{x},\mathbf{y}) = -6(x_i - y_i)(x_j - y_j)(x_k - y_k)/|\mathbf{x} - \mathbf{y}|^5$ is the Stresslet singularity, $\hat{\mathbf{n}}$ is the outward pointing unit normal vector, and $\mathbf{q}(\mathbf{y})$ and $\mathbf{h}(\mathbf{y})$ are unknown Stresslet densities. In the limit as the point $\mathbf{x}$ is taken to a point $\mathbf{x}^S$ on the helical or cylindrical container boundary, the no-slip boundary condition reveals equations for the unknown densities $\mathbf{q}$ and $\mathbf{h}$. The fluid velocity on the helical boundary at a point $\mathbf{x}^S$ is given by $U\hat{\mathbf{z}} + \Omega\,\hat{\mathbf{z}} \times \mathbf{x}^S + \mathbf{u}'(\mathbf{x}^S)$, where

$$\mathbf{u}'(\mathbf{x}^S(\theta,\zeta)) = -\varepsilon f'(\theta)\,[\cos(\nu^*\zeta + \theta)\,\hat{\mathbf{x}} + \sin(\nu^*\zeta + \theta)\,\hat{\mathbf{y}}] \tag{10}$$

denotes the velocity of the helical wave from Eq. (3). After some manipulation, for a point $\mathbf{x}^S$ a point on the helical boundary, Eq. (9) tends to the form

$$U\hat{\mathbf{z}} + \Omega\,\hat{\mathbf{z}} \times \mathbf{x}^S + \mathbf{u}'(\mathbf{x}^S) = \int_{\partial S} \big(\mathbf{q}(\mathbf{y}) - \mathbf{q}(\mathbf{x}^S)\big) \cdot \mathbf{T}(\mathbf{x}^S,\mathbf{y}) \cdot \hat{\mathbf{n}}(\mathbf{y})\, dS_y + \int_{\partial S_C} \mathbf{h}(\mathbf{y}) \cdot \mathbf{T}(\mathbf{x}^S,\mathbf{y}) \cdot \hat{\mathbf{n}}(\mathbf{y})\, dS_y. \tag{11}$$

Meanwhile, in the limit as the point $\mathbf{x}$ is taken to a point $\mathbf{x}^C$ on the cylindrical container, we have (using the no-slip condition)

$$\mathbf{0} = \int_{\partial S} \mathbf{q}(\mathbf{y}) \cdot \mathbf{T}(\mathbf{x}^C,\mathbf{y}) \cdot \hat{\mathbf{n}}(\mathbf{y})\, dS_y + 8\pi\mathbf{h}(\mathbf{x}^C) + \int_{\partial S_C} (\mathbf{h}(\mathbf{y}) - \mathbf{h}(\mathbf{x}^C)) \cdot \mathbf{T}(\mathbf{x}^C,\mathbf{y}) \cdot \hat{\mathbf{n}}(\mathbf{y})\, dS_y, \tag{12}$$

where the extra factor of $8\pi\mathbf{h}(\mathbf{x}^C)$ is a consequence of the jump discontinuity of the Stresslet singularity across the boundary.[61]

The nullspace of the double layer integral operator is six-dimensional, corresponding to the six modes of rigid body translation and rotation. The helical symmetry of the body assures that both the possible translation and rotation are only one-dimensional, but conditions must be placed on the density $\mathbf{q}$ so that the Fredholm alternative assures a unique solution to Eqs. (11) and (12). The details involve an application of Weilandt's deflation technique (see Refs. 61 and 62), and the relations that result close the system

$$-\frac{4\pi}{S_A}\int_{\partial S} \mathbf{q}(\mathbf{y})\, dS_y = U\hat{\mathbf{z}}, \quad -4\pi\sum_{m=1}^{3}\frac{1}{A_m}\mathbf{e}_m\left(\mathbf{e}_m \cdot \int_{\partial S} \mathbf{y} \times \mathbf{q}(\mathbf{y})\, dS_y\right) = \Omega\,\hat{\mathbf{z}}, \tag{13}$$

where S_A is the surface area of the helical body, $A_m = \int_{\partial S} |(\mathbf{e}_m \times \mathbf{y})|^2\, dS_y$, and $\mathbf{e}_m$ is the mth Cartesian unit vector. Equations (11)–(13) together form a closed system for $\mathbf{q}$, $\mathbf{h}$, U, and Ω. Only minor modifications are necessary for computing the flow internal to a helical body. In that case, we specify the boundary velocity $\mathbf{u}'(\mathbf{x}^S)$ completely, and we solve

$$\mathbf{u}'(\mathbf{x}^S) = 8\pi\mathbf{q}(\mathbf{x}^S) + \int_{\partial S} (\mathbf{q}(\mathbf{y}) - \mathbf{q}(\mathbf{x}^S)) \cdot \mathbf{T}(\mathbf{x}^S,\mathbf{y}) \cdot \hat{\mathbf{n}}(\mathbf{y})\, dS_y \tag{14}$$

for the density $\mathbf{q}$. The internal flow field is then recovered using Eq. (9) with $\mathbf{h} = 0$.

Using the helical symmetry in the problem, the density $\mathbf{q}$ (and $\mathbf{h}$ in the external problem) is given by a translation and rotation through space given their values in the $x - y$ plane; for example,

$$\mathbf{q}(\mathbf{y}(\theta,\zeta)) = \mathbf{R}(\zeta;\nu)\,\mathbf{q}_0(\theta), \tag{15}$$

$$\mathbf{R}(\zeta;\nu) = \begin{pmatrix} \cos(\nu\zeta) & -\sin(\nu\zeta) & 0 \\ \sin(\nu\zeta) & \cos(\nu\zeta) & 0 \\ 0 & 0 & 1 \end{pmatrix}, \tag{16}$$

where $\mathbf{q}_0(\theta) = \mathbf{q}(\mathbf{y}(\theta,\zeta=0))$. The angle θ is discretized uniformly on $[0,2\pi)$ by setting $\theta_j = 2\pi(j-1)/M$ for $j \in \{1,\ldots,M\}$. A Nyström collocation method is employed (see Ref. 63) in which integral equation (11) is assumed to hold at the quadrature nodes, $\mathbf{x}^S = \mathbf{y}(\theta_j,\zeta=0)$. This produces a linear system of equations for the density at the nodes, $\mathbf{q}_0(\theta_j)$ and $\mathbf{h}_0(\theta_j)$, the swimming speed U, and the rigid body rotation rate, Ω. The surface integrals in Eqs. (11) and (12) are performed by truncating the integrals at a finite number of wavelengths, N_W, and discretizing the axial variable $\zeta \in [-N_W\pi/\nu, N_W\pi/\nu]$ at the points corresponding to the Gaussian quadrature nodes, ζ_j, with $j = 1,\ldots,N_W$.

Integrals in θ and ζ are performed with high-order accuracy using Gaussian quadrature.[64] The azimuthal resolution M, the axial resolution N_A, and the number of wavelengths N_W are chosen so that further increases change the resulting velocities by less than 0.5% in every case considered. Similar methods have been used to study helical swimming in Stokes flow,[65] inside a capillary tube,[49] and in viscoelastic flow.[51] We refer the reader to Ref. 59 for a validation of the code.

III. EXTERNAL STOKES FLOW

We begin our analytical investigation by studying the "external" problem: the swimming of a helical body inside a cylindrical tube of dimensionless radius L. The problem of swimming in an unconfined domain will be solved by taking the limit $L \to \infty$. First, the dimensionless Stokes equations, Eq. (4), may be transformed into the helical coordinate system as follows:

$$\frac{\partial p}{\partial r} = \frac{1}{r}\frac{\partial}{\partial r}\left(r\frac{\partial u}{\partial r}\right) - \frac{u}{r^2} - \frac{2}{r^2}\frac{\partial v}{\partial \theta} + \frac{1}{r^2}\frac{\partial^2 u}{\partial \theta^2} + \nu^2\frac{\partial^2 u}{\partial \theta^2}, \tag{17}$$

$$\frac{1}{r}\frac{\partial p}{\partial \theta} = \frac{1}{r}\frac{\partial}{\partial r}\left(r\frac{\partial v}{\partial r}\right) - \frac{v}{r^2} + \frac{2}{r^2}\frac{\partial u}{\partial \theta} + \frac{1}{r^2}\frac{\partial^2 v}{\partial \theta^2} + \nu^2\frac{\partial^2 v}{\partial \theta^2}, \tag{18}$$

$$-\nu\frac{\partial p}{\partial \theta} = \frac{1}{r}\frac{\partial}{\partial r}\left(r\frac{\partial w}{\partial r}\right) + \frac{1}{r^2}\frac{\partial^2 w}{\partial \theta^2} + \nu^2\frac{\partial^2 w}{\partial \theta^2}, \tag{19}$$

$$\frac{\partial u}{\partial r} + \frac{u}{r} + \frac{1}{r}\frac{\partial v}{\partial \theta} - \nu\frac{\partial w}{\partial \theta} = 0, \tag{20}$$

and the no-slip boundary condition for the torque-free helical body is $\mathbf{u}(\mathbf{x}^S) = -\varepsilon f'(\theta)\hat{\mathbf{r}} + \Omega(1+\varepsilon f(\theta))\hat{\boldsymbol{\theta}} + U\hat{\mathbf{z}}$ (see Eq. (3)). Our approach will be to decompose the problem into two subproblems, to be solved in succession. In the first problem, the helical wave is assumed to propagate on a non-rotating cylindrical base, $\Omega = 0$, which results in a force-free swimming speed U_w (w for "wave"), which we determine up to second order in the small wave amplitude using a regular perturbation expansion and to fourth order using a double series expansion in the inner problem of an asymptotic matching calculation. However, this flow also produces a torque on the body, so to study force- and torque-free swimming, we solve a second problem in which the torque is balanced by a rigid body rotation with rate Ω. This problem, however, was solved in our previous paper (in the unbounded case), and the results are reproduced here. This second solution for rigid body rotation corresponds to another swimming speed, U_r (r for "rotation"), so that the final force- and torque-free swimming speed is $U = U_w + U_r$ by the linearity of the Stokes equations.

A. Contribution from the helical wave

Denoting again the helical surface as ∂S, and recalling that the outer cylindrical boundary has radius L, the boundary conditions in the problem with $\Omega = 0$ fixed are

$$\mathbf{u}(\mathbf{x} \in \partial S) = -\varepsilon f'(\theta)\hat{\mathbf{r}} + U_w\hat{\mathbf{z}}, \quad \mathbf{u}(r=L) = \mathbf{0}. \tag{21}$$

With ε assumed small, we consider a regular perturbation expansion of the velocity, pressure, and swimming speed,

$$p = p_0 + \varepsilon p_1 + \varepsilon p_2 + O(\varepsilon^3), \quad U_w = \varepsilon U_1 + \varepsilon^2 U_2 + O(\varepsilon^3), \quad \mathbf{u} = \varepsilon \mathbf{u}_1 + \varepsilon^2 \mathbf{u}_2 + O(\varepsilon^3), \tag{22}$$

where p_0 is set to 0 without loss of generality and we write $\mathbf{u}_m = u_m \hat{\mathbf{r}} + v_m \hat{\boldsymbol{\theta}} + w_m \hat{\mathbf{z}}$. The boundary conditions up to second order are determined by Taylor expansion of Eq. (21) (note that the base cylinder in the dimensionless system is located at $r = 1$), giving

$$u_1(1,\theta) = -f'(\theta), \quad v_1(1,\theta) = 0, \quad w_1(1,\theta) = U_1, \tag{23}$$

$$u_2(1,\theta) = -f(\theta)\frac{\partial u_1(1,\theta)}{\partial r}, \quad v_2(1,\theta) = -f(\theta)\frac{\partial v_1(1,\theta)}{\partial r}, \quad w_2(1,\theta) = U_2 - f(\theta)\frac{\partial w_1(1,\theta)}{\partial r}. \tag{24}$$

Note that if the profile is described by a single Fourier mode, $f(\theta) = \cos(N\theta)$, then the operation $\varepsilon \to -\varepsilon$ is equivalent to a phase shift in $f(\theta)$, and there is no change in the dynamics. We can therefore expect the swimming speed to appear only in even powers of ε, so that the swimming speed must enter only as $O(\varepsilon^2)$. In fact, the swimming speed must enter at $O(\varepsilon^2)$ for general $f(\theta)$. Since the system is linear in the wave profile at $O(\varepsilon)$ (it is not linear at $O(\varepsilon^2)$ and beyond), the swimming speed can be decomposed into a superposition of each Fourier mode, and for each Fourier mode, the phase-shift argument above applies.

We will consider a Fourier series expansion for the wave profile,

$$f(\theta) = \sum_k \hat{f}_k e^{ik\theta}, \tag{25}$$

and without loss of generality, we will take $\hat{f}_0 = 0$. The pressure and velocity components are similarly expressed; for example, $u_m = \sum_k \hat{u}_{mk} e^{ik\theta}$. Before stepping through the problem order by order in ε, first note that the general forms for the $k = 0$ mode part of the flow are found by integrating the Stokes equations directly, which are made much simpler for $k = 0$ since all of the θ dependent terms and derivatives in Eqs. (17)-(20) vanish. The resulting forms are

$$\hat{p}_{m0}(r) = \text{const.}, \ \hat{u}_{m0}(r) = 0, \ \hat{v}_{m0}(r) = \hat{v}_{m0}(1)\frac{1/r - r/L^2}{1 - 1/L^2}, \ \hat{w}_{m0}(r) = \hat{w}_{m0}(1)\left(1 - \frac{\ln r}{\ln L}\right). \tag{26}$$

Consider now the leading order dynamics at $O(\varepsilon)$. At this order, the system decouples into the dynamics associated with each individual mode of $f(\theta)$, and the solution is given by a superposition of each mode of the flow. By the boundary conditions and the force-free condition, the velocity field for $k = 0$ at this order and U_1 are therefore zero since $\hat{f}_0 = 0$. For the remaining modes, we may write

$$\hat{p}_{1k} = \mathscr{P}_k \hat{f}_k, \quad \hat{u}_{1k} = \mathscr{U}_k \hat{f}_k, \quad \hat{v}_{1k} = \mathscr{V}_k \hat{f}_k, \quad \hat{w}_{1k} = \mathscr{W}_k \hat{f}_k, \tag{27}$$

so that $(\mathscr{P}_k, \mathscr{U}_k, \mathscr{V}_k, \mathscr{W}_k)\exp(ik\theta)$ is a solution to the Stokes equations, Eqs. (17)-(20). Defining $q = |k|$ and $\lambda = q\nu r$, by the same approach as in Ref. 59, we find $\mathscr{P}_k$ and $\mathscr{W}_k$,

$$\mathscr{P}_k = -ika_q K_q(\lambda) - ikb_q I_q(\lambda), \tag{28}$$

$$\mathscr{W}_k = \frac{a_q}{2\nu}\lambda K_{q-1}(\lambda) - \frac{b_q}{2\nu}\lambda I_{q-1}(\lambda) + c_q K_q(\lambda) + d_q I_q(\lambda), \tag{29}$$

where I_q and K_q are the modified Bessel functions of the first and second kind, respectively, and the coefficients a_q, b_q, c_q, d_q are determined by the boundary conditions

$$\mathscr{W}_k(r = 1) = 0, \quad \mathscr{W}_k(r = L) = 0, \quad \mathscr{U}_k(r = 1) = -ik, \tag{30}$$

$$\mathscr{U}_k(r = L) = 0, \quad d\mathscr{U}_k/dr|_{r=1} = ik, \quad d\mathscr{U}_k/dr|_{r=L} = 0. \tag{31}$$

The boundary conditions for $d\mathscr{U}_k/dr$ are found using the incompressibility condition (20). The resulting linear system for the coefficients (along with two extra coefficients introduced in the expression for $\mathscr{U}_k$, which is given in Appendix A) may be solved in a straightforward way, though the final expressions are long and complicated and we refrain from listing them here. However, the limit $L \to \infty$ (unconfined swimming) reveals simpler expressions, since the I_q components of the

flow must vanish as they are unbounded at infinity. The analytical solutions in that case are given by

$$\mathscr{P}_k = -ikA_qK_q(\lambda), \tag{32}$$

$$\mathscr{W}_k = \frac{A_q}{2\nu}\left(\lambda K_{q-1}(\lambda) - \frac{q\nu K_{q-1}(q\nu)}{K_q(q\nu)}K_q(\lambda)\right), \tag{33}$$

while the constants A_q are given by (recall that $q = |k|$)

$$A_q = \frac{2\left(q + \dfrac{q\nu K_{q-1}}{K_q}\right)}{qK_q + q\nu K_{q-1} - \dfrac{2(q-2)}{\nu}K_{q-1} - \dfrac{(3q-2)K_{q-1}^2}{K_q} - \dfrac{q\nu K_{q-1}^3}{K_q^2}}, \tag{34}$$

where $K_{q-1} = K_{q-1}(q\nu)$ and $K_q = K_q(q\nu)$. Defining $J_q = d\mathscr{W}_q/dr$ for notational convenience, we find that

$$J_q = \frac{q^2a_q}{2}\left(K_{q-1} - \nu K_q\right) - \frac{q^2b_q}{2}\left(I_{q-1} + \nu I_q\right) - c_qq\left(K_q + \nu K_{q-1}\right) - d_qq\left(I_q - \nu I_{q-1}\right), \tag{35}$$

where all Bessel functions without any argument are evaluated at $q\nu$, which in the limit of swimming in an unconfined fluid (as $L \to \infty$) is given by

$$J_q = \frac{q^2A_q}{2}\left(2K_{q-1} - \nu K_q + \frac{\nu K_{q-1}^2}{K_q}\right). \tag{36}$$

With the solutions at $O(\varepsilon)$ in hand, the swimming speed at $O(\varepsilon^2)$ may be found immediately using the boundary condition $\hat{w}_{20}(1) = U_2 - \sum_k |\hat{f}_k|^2 d\mathscr{W}_k(1)/dr$, from Eq. (24). But, the spatially averaged axial flow on the boundary at second order, $\hat{w}_{20}(1)$, can be determined rapidly by investigation of the fluid force on the body. The force per unit length is found by integrating the fluid stress around a cross section, and up to $O(\varepsilon^2)$ is given by (see Appendix B)

$$\mathscr{F}_w = 2\pi\varepsilon^2\frac{d\hat{w}_{20}}{dr}\Big|_{r=1}. \tag{37}$$

Using Eq. (26), force-free swimming therefore requires that $\hat{w}_{20}(1) = 0$, so that the $O(\varepsilon^2)$ value of the swimming speed is given by

$$U_w = 2\varepsilon^2\sum_{q\geq 1}|\hat{f}_q|^2J_q. \tag{38}$$

In our previous work, we carried a similar calculation to the one above out to fourth order in the small wave amplitude assuming only a single mode for the boundary, $f(\theta) = \cos(N\theta)$, using a double-series expansion in $\delta = \varepsilon\nu$ and ν^{-1}.[59] This was made necessary by a boundary layer of thickness $O(\nu^{-1})$ in the fluid near the helical surface for small helical pitches (large ν). A similar boundary layer appears in the problem of present interest as well. The boundary layer is due to the factor of ν which appears with the derivative $\partial/\partial\theta$ in Eqs. (17)-(20), reflecting a fast variation of the boundary condition along the z direction via Eq. (7). Balancing terms, we notice that $\partial/\partial r \sim \nu\,\partial/\partial\theta$ which suggests the presence of a boundary layer of thickness $O(\nu^{-1})$ near the helical body surface inside which the flow varies rapidly. Outside of the boundary layer, the solution is very close to the solution for a cylindrical body, which in our problem here is a motionless fluid. Investigating the inner solution by the double series technique used in Ref. 59, but applied instead to the helical wave boundary condition above, the correction at $O(\varepsilon^4)$ is found to be

$$U_w = \frac{\varepsilon^2}{2}J_N + \varepsilon^4\left(-\frac{1}{2}\nu^3N^4 + \nu^2\frac{3}{8}N^3\right) + O\left(\varepsilon^4\nu + \varepsilon^6\nu^6\right), \tag{39}$$

and note that the asymptotic form of the swimming speed in the large ν regime is given by

$$U_w \approx \varepsilon^2\left(\frac{1}{2}N^2\nu - \frac{1}{2}N\right) + \varepsilon^4\left(-\frac{1}{2}\nu^3N^4 + \nu^2\frac{3}{8}N^3\right) + O\left(\varepsilon^4\nu + \varepsilon^6\nu^6\right). \tag{40}$$

If ν is large enough, since the boundary layer around $r = 1$ has thickness $O(\nu^{-1})$, the velocity field in the radially confined problem tends towards the velocity field in the unconfined problem. Hence, the asymptotic correction for large ν is identical in both the confined and unconfined problems. On the other hand, if ν is small and ν^{-1} is comparable with $L - 1$, the outer boundary plays a significant role, as we will discuss shortly. In this case, since ν^{-1} is not small, a boundary layer analysis is unnecessary and the solutions at $O(\varepsilon^2)$ are sufficiently accurate.

For increasing ν (decreasing pitch angle), the boundary actuation tends to appear as though waves are passing directly downward axially, and the dynamics may be compared to the expressions for Taylor's infinite swimming sheet.[20] In the present setting, writing the wave profile as $\rho = 1 + \varepsilon\cos(N\varphi - N\nu\zeta - Nt)$, the corresponding infinite sheet is described by $\tilde{y} = \tilde{\varepsilon}\cos(\tilde{x} + \tilde{t})$ and swims with speed $\tilde{U} = \tilde{\varepsilon}^2/2$, where we identify $\tilde{\varepsilon} = N\nu\varepsilon$, $\tilde{x} = N\nu\zeta$, $\tilde{t} = Nt$, and $\tilde{U} = \nu U$. The Taylor-sheet prediction for such boundary motion in the present variables would then be $U = (2\nu)^{-1}(N\nu\varepsilon)^2$, which agrees precisely with the asymptotic form above.

Meanwhile, the torque per unit length up to $O(\varepsilon^2)$ is given by

$$\mathcal{L}_w = 2\pi\varepsilon^2\left(\frac{d\hat{v}_{20}}{dr} - \hat{v}_{20}\right)_{r=1} = \frac{-4\pi\varepsilon^2}{1 - 1/L^2}\hat{v}_{20}(1) = \frac{4\pi\varepsilon^2}{1 - 1/L^2}\sum_k |\hat{f}_k|^2 \mathscr{V}_k'(1), \tag{41}$$

using Eq. (26) and the boundary condition in Eq. (24) (see Appendix B). The boundary value $\mathscr{V}_k'(1)$ may be determined by taking a derivative of the incompressibility condition and using Eq. (17) and is again a complicated expression for general L. However, for $L = \infty$, the expression reduces to

$$\mathscr{V}_k'(1) = A_q \nu q\left((q-1)K_{q-1} - \left(\frac{1}{2}q\nu + \frac{1}{\nu}\right)K_q + \frac{q\nu}{2}\frac{K_{q-1}^2}{K_q}\right) + q^2(\nu^2 + 1), \tag{42}$$

where A_q is given in Eq. (34) and $K_{q-1} = K_{q-1}(q\nu)$ and $K_q = K_q(q\nu)$ as before. For the case of torque-free swimming, an extra rigid body rotation must balance this torque, which is the topic of Sec. III B. The results in the case of an unconfined domain are consistent with the $L \to \infty$ limits.

B. Torque-balancing rigid body rotation

The helical wave discussed in Sec. III A introduces a net torque on the body, so to solve the problem of torque-free swimming, we must introduce an extra rigid body rotation to drive surface motion opposite the direction of helical wave passage. The mobility relation of rigid body rotation and torque for the helical bodies studied here was the focus of our previous work, where a similar approach as in Sec. III A was applied.[59]

At leading order in the small amplitude ε, the fluid velocity due to rigid body rotation with rate Ω is a purely axisymmetric flow,

$$\mathbf{u}^{(r)} = \Omega\,\frac{1/r - r/L^2}{1 - 1/L^2}\hat{\boldsymbol{\theta}} + O(\varepsilon\Omega), \tag{43}$$

and the torque generated by the rigid body motion is given by (for axisymmetric flow around a cylinder)

$$\mathcal{L}_r = 2\pi\left(\frac{\partial v^{(r)}}{\partial r} - v^{(r)}\right)_{r=1} + O(\varepsilon\Omega). \tag{44}$$

Balancing $\mathcal{L}_r$ with $\mathcal{L}_w$ from Eq. (41), we find the torque-balancing rigid body rotation rate for all values of the outer container radius L,

$$\Omega = 2\varepsilon^2\sum_{q\geq 1}|\hat{f}_q|^2\mathscr{V}_q'(1) + O(\varepsilon^3). \tag{45}$$

The rotation rate scales as $O(\varepsilon^2)$. However, the swimming speed due to rigid body rotation is given by $U_r = C\varepsilon^2\Omega$, for a shape dependent coefficient C with $C = O(1)$ (see Ref. 59). Therefore, the adjustment to the swimming speed due to the compensating rigid body rotation only enters

at $O(\varepsilon^4)$, so to second order accuracy in ε, the torque-free swimming speed is given simply by $U = U_w + U_r \approx U_w$, with U_w given in Eq. (38).

For a boundary described by a single mode, $f(\theta) = \cos(N\theta)$, with $N \geq 2$, the rotation rate Ω is negative (intuitively, the compensating rigid body rotation acts in the direction opposing the helical wave motion to satisfy torque balance). However, for $N = 1$, the rotation rate can be positive for sufficiently small helical pitch (small ν). We will return to this surprising result in Sec. III C.

In the case that $f(\theta) = \cos(N\theta)$, another conclusion from the large ν boundary layer analysis is that $\hat{v}_{20} = O(\nu^0)$. (Moreover, numerical values of the expression above strongly suggest that $\hat{v}_{20} \sim N^2\nu^0$ and $\Omega = O\left(\varepsilon^2\nu^0\right)$ as ν becomes large.) As shown in Ref. 59, the speed by rigid rotation has the asymptotic expression

$$U_r = \Omega\,\varepsilon^2\left(N - \frac{3}{2}\nu^{-1}\right) = \varepsilon^4 \cdot O\left(\nu^0\right). \tag{46}$$

Upon investigation of Eq. (39), for large ν, the swimming speed due to the helical wave motion scales as ν^3 in the fourth order correction, which is much larger than the correction above. Therefore, the effect of rigid body rotation is negligible even in the asymptotic correction at $O(\varepsilon^4)$ in the case of a single Fourier mode boundary profile and in the large ν (small pitch angle) regime.

C. Comparison of analytical and numerical results

The analytical expressions for the swimming speed are expected to be valid for small wave amplitude, ε, for large helical pitch, $2\pi/\nu$, and for relatively small wave numbers describing the helical cross section, N (since N can be seen roughly to modify the effective helical pitch). In order to see where the analytical expressions are valid and where they break down, we compare the analytical expressions found in Secs. III A and III B to full numerical simulations using the method described in Sec. II B. Figure 3(a) shows the normalized swimming speeds, U/ε^2, in an infinite fluid domain for the first four individual Fourier modes describing the boundary, $f(\theta) = \cos(N\theta)$, and over a wide range of ν, with $\varepsilon = 0.025$ fixed. The computed values are shown as symbols, the $O(\varepsilon^2)$ estimates are shown as dashed lines, and the $O(\varepsilon^4)$ predictions are shown as solid lines. The analytical expressions agree exceptionally well with the numerically determined values for the range of parameters studied. The swimming speed is monotonic in the wave number N in this regime, and the analytical estimates are more accurate for smaller values of N as expected.

In the study of swimming by rigid body rotations in an unbounded fluid, a speed maximizing value of ν was found in the range considered here, and the $O(\varepsilon^4)$ correction was used to select this value of ν.[59] It is interesting to note the difference in this case, in that the computed values of the swimming speed are monotonic in ν, at least in the range of ν considered, and we expect that they will continue to increase and tend towards the "Taylor swimming sheet" value, $U/\varepsilon^2 \sim N^2\nu/2$, as discussed in Sec. III A.

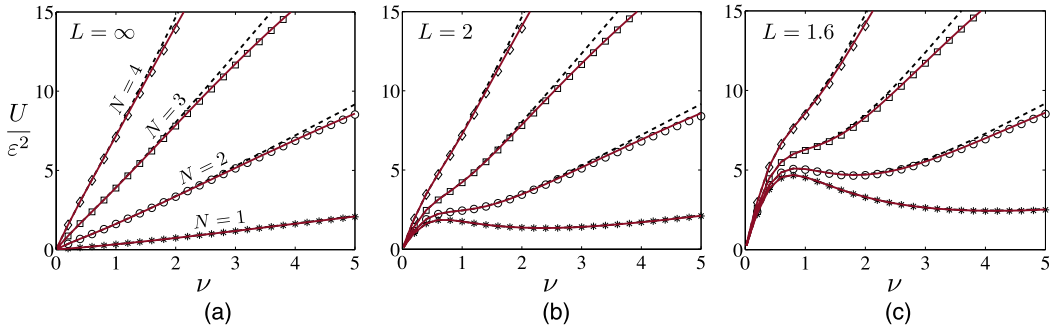

FIG. 3. The normalized swimming speed U/ε^2 as a function of ν for $N = 1$ (stars), 2 (circles), 3 (squares), and 4 (diamonds) with $\varepsilon = 0.025$ fixed. Dashed lines correspond to the $O(\varepsilon^2)$ theory, while solid lines correspond to the $O(\varepsilon^4)$ theory. (a) Infinite domain; (b) radially confined domain with $L = 2$; (c) radially confined domain with $L = 1.6$.

Figure 3(b) shows the computed values and the $O(\varepsilon^2)$ and $O(\varepsilon^4)$ estimates of the normalized swimming speed, but now for swimming inside a cylindrical tube of dimensionless radius $L = 2$ (recall the dimensionless base cylinder for the swimming body has radius 1). The analytical expressions are still very accurate for sufficiently small values of ν. The computed values show that the effect of the confined domain is more pronounced for smaller N and smaller ν. Particularly for small values of ν (large helical pitch), the presence of the outer container is found to significantly increase the swimming speed. Figure 3(c) shows the comparison again but now for an even tighter boundary geometry, $L = 1.6$. Now the increase in the swimming speed for small ν is dramatic, as is the non-monotonicity of the swimming speed in ν: local maxima and minima in the swimming speed are now observed for $N = 2$ as well as for $N = 1$ in the range shown, and there is a plateau of speeds for the $N = 3$ case for a wide range in ν.

To better understand the effect of confinement on the swimming speed, recall that the width of boundary layer near the helical body scales as $O(\nu^{-1})$. When ν is small, the boundary layer extends to the region near the outer cylindrical boundary, so that the swimming speed may be affected by its presence. In particular, the flow which otherwise was translating axially opposite the direction of swimming must now satisfy the no-slip condition on the wall, effectively providing an extra force on the body which increases its swimming speed. As the helical pitch decreases (as ν increases), the boundary layer draws inward towards the helical surface and the effect of the outer boundary diminishes. In fact, the effect of the outer tube diminishes exponentially fast with the tube diameter; the asymptotic form of flow can be shown in the boundary layer analysis to scale as $\exp(-N\nu(r-1))$, and the swimming speed rapidly relaxes to its value in an infinite fluid with increasing $N\nu$. With these effects combined, the swimming speed can exhibit local maxima and minima in the helical pitch when the body is confined in a cylindrical tube.

Figure 4 shows how the swimming speed changes as a function of the radius of the cylindrical container, L, indicating more clearly how the swimming speed by helical wave propagation is enhanced when the body is confined in a cylindrical tube. The normalized speed U/ε^2 is shown with $N = 2$ and $\varepsilon = 0.075$ fixed and for $\nu = 1$ and $\nu = 2$. While the smaller of the two helical pitches leads to faster swimming in an infinite fluid, the larger of the two helical pitches leads to faster swimming in a confined domain. As L tends towards 1, where the helical body is almost perfectly contained, our analytical predictions are not expected to hold. Figure 4 is somewhat misleading as it suggests that the swimming speed will continue to increase without bound for further decreases in L, but this is clearly unphysical. A numerical investigation by Liu *et al.* for slender helical bodies in

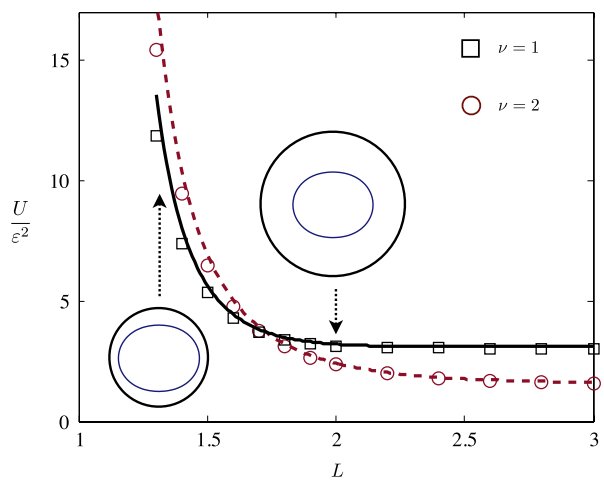

FIG. 4. The normalized swimming speed U/ε^2 for different outer radii L, with $\varepsilon = 0.075$ and $N = 2$ fixed. The dashed/solid lines show the analytical results for $\nu = 1$ and $\nu = 2$. Circles and squares indicate the corresponding values computed by full numerical simulations. The effect of confinement is a dramatic increase in the swimming speed for helical wave swimming, though the limit is assured to be finite as $L \to 1$.

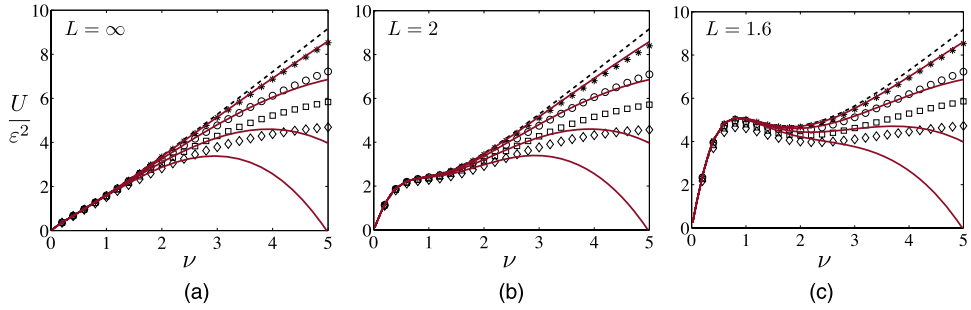

FIG. 5. The normalized swimming speed U/ε^2 as a function of ν for $\varepsilon = 0.025$ (stars), 0.05 (circles), 0.075 (squares), and 0.1 (diamonds) with $N = 2$ fixed. Dashed/solid lines correspond to the $O(\varepsilon^2)$ and $O(\varepsilon^4)$ theories. (a) Infinite domain; (b) radially confined domain with $L = 2$; (c) radially confined domain with $L = 1.6$.

a cylindrical tube showed an increase in the speed but then a maximum and a decrease in the speed over a very small region of the tube radius nearing total confinement.[49]

Recently, Felderhof[46] studied swimming by the passage of single-mode helical waves in a circular tube and found the swimming speed accurate to second order. Our results agree with his in the single-mode case for small ε and large ν (ka in Ref. 46): namely, the swimming speed increases to a local maximum and then decreases, and the rotation rate enters at $O(\varepsilon^2)$, but by analyzing the dynamics for larger pitch angles, we now see the recovery of increasing speeds with increasing ν.

Instead of fixing ε, we may fix N and explore the validity of the analytical estimates as ε is increased. Figures 5(a)-5(c) show how varying ε affects the U/ε^2-ν relations with $N = 2$ fixed, again for unconfined swimming, confined swimming with $L = 2$, and then again with $L = 1.6$. The $O(\varepsilon^2)$ theory predicts a curve that is independent of ε but the computed values show a significant deviation from the prediction (dashed line) with increasing ν, so that the correction at $O(\varepsilon^4)$ is necessary to reflect this deviation. For $\varepsilon = 0.025$, with the fourth order correction, the theory now agrees very well with the numerics for the range of ν considered. For larger values of ε, the fourth order correction only improves the accuracy for relatively small values of ν. Revisiting Eq. (39), we expect the estimation of U/ε^2 to become invalid when $\varepsilon^2\nu$ is large. When the body is moving in a more tightly confined environment, as shown in Fig. 5(c) for $L = 1.6$, the small amplitude expansion appears inaccurate when $\varepsilon/(L-1)$ is large; i.e., when the amplitude of the perturbation, ε, is comparable with the width of the fluid domain, $L - 1$. The approximation could be improved by computing yet higher orders of the Taylor expansion in ε, as was performed for Taylor's swimming sheet by Sauzade *et al.*[66]

Finally, Fig. 6 shows the torque-balancing rigid body rotation rate for a single Fourier mode boundary geometry, as determined by numerical simulations (symbols) and the analytical values from Eq. (45) (dashed lines). Once again we include a comparison between motion in an unconfined domain and in confined domains with outer tube radii $L = 2$ and $L = 1.6$. The analytical results

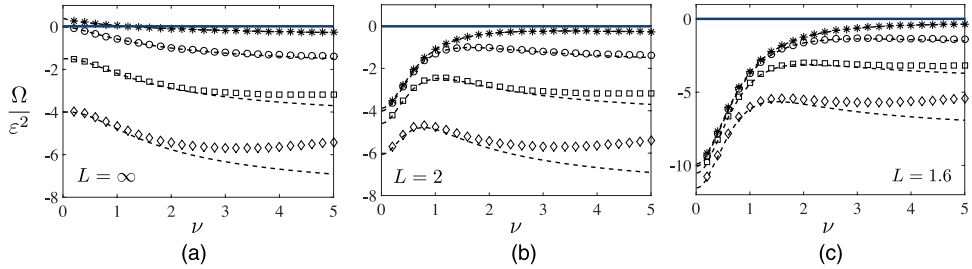

FIG. 6. The normalized torque-balancing rigid body rotation rate, Ω/ε^2 as a function of ν for $N = 1$ (stars), 2 (circles), 3 (squares), and 4 (diamonds) with $\varepsilon = 0.025$ fixed. Dashed lines correspond to the $O(\varepsilon^2)$ theory. (a) Infinite domain; (b) radially confined domain with $L = 2$; (c) radially confined domain with $L = 1.6$. $\Omega = 0$ is shown as a solid line.

generally agree very well with the numerical results for the range of helical pitch shown, with accuracy diminishing in the $N = 4$ case for large ν. Intuitively, the compensating rigid body rotation rate is almost always negative, opposing the direction of wave passage along the surface of the helical body. However, in the case of unconfined swimming for $N = 1$ and ν less than approximately 1.3, we find surprisingly that the compensating rotation rate is in fact positive; i.e., the torque-balancing rotation is in the same direction as the passing wave. For nearly all body and wave geometries considered, the surface dynamics locally are similar to that of the classical transversely waving Taylor swimming sheet,[20] which swims opposite the direction of the wave. However, Taylor also considered the motion of sheet along which waves pass longitudinally, which instead swims in the same direction as the wave. This may relate to the reversal of the torque-balancing rotation direction, though the effect would be subtle since the swimming speed does not change sign for any helical wave geometry.

The presence of an outer tube increases the magnitude of the compensating rotation rate, suggesting an extra torque on the body from the requirement of the no-slip condition on the outer surface, just as there was an apparent extra force due to the container that led to increased swimming speeds. The peculiar positive rotation rate for $N = 1$ and small ν vanishes in the confined problem once L is sufficiently small.

IV. INTERNAL STOKES FLOW

We have analyzed and computed the fluid flow and accompanying force- and torque-free swimming of helical bodies in the external problem. Now, using only a slight modification of the analysis above, we solve for the pumping flow internal to the helical body driven by the passage of the same helical waves. The internal flow due to rigid body rotation is uninteresting—the fluid simply moves as a rigid body along with the boundary motion. However, the internal flow due to the passage of helical waves on the surface can be quite intricate. We now consider the problem where the base cylinder neither rotates nor translates, and material points on the body surface move in fixed periodic orbits in space, so that the velocity boundary conditions are given by

$$\mathbf{u}(\mathbf{x} \in \partial S) = -\varepsilon f'(\theta)\hat{\mathbf{r}}, \quad \mathbf{u}(\mathbf{x} \to 0) \text{ is finite}, \tag{47}$$

where ∂S still denotes the helical surface which is now the outer boundary of the fluid domain.

The pumping rate is defined as the mean flow through a cross section of the helical domain,

$$R(\varepsilon) = -\int_0^{2\pi}\int_0^{1+\varepsilon f(\theta)} \sum_{n\geq 1} \varepsilon^n w_n(r,\theta)\, r\, dr\, d\theta, \tag{48}$$

defined to be positive if the mean flow is in the $-\hat{\mathbf{z}}$ direction. Using the exact boundary condition $\sum_n \varepsilon^n w_n|_{r=1+\varepsilon f(\theta)} = 0$ and Eq. (23) (in this case $U_1 = 0$), we obtain $R'(0) = 0$, $R''(0) = -4\pi \int_0^1 r\, \hat{w}_{20} dr$, and thus

$$R(\varepsilon) = -2\pi\varepsilon^2 \int_0^1 r\hat{w}_{20}(r)\, dr + O(\varepsilon^3). \tag{49}$$

The internal pumping rate accurate to $O(\varepsilon^2)$ requires only the determination of $\hat{w}_{20}(r)$. However, note that the $k = 0$ mode of the flow structure is again found easily by removing the θ dependence of the Stokes equations, Eqs. (17)-(20), and integrating, revealing

$$\hat{p}_{m0} = \text{const.}, \quad \hat{u}_{m0} = 0, \quad \hat{v}_{m0} = \hat{v}_{m0}(1)r, \quad \hat{w}_{m0}(r) = \hat{w}_{m0}(1), \tag{50}$$

so in fact the mean flow $\hat{w}_{20}(r)$ is constant throughout the domain. In addition, the torque on the boundary due to the internal flow is given by Eq. (41) up to a negative sign. Thus, unlike in the external problem, the torque in the internal problem at $O(\varepsilon^2)$ is 0, since $\hat{v}_{20}$ is linear in r. Similarly, we find that the force at this order is zero since $\hat{w}_{20}$ is a constant. In fact, we can say more. Consider a non-rotating cylinder on which the helical waves are passed. Assuming that the force-free swimming speed is V, we write the boundary condition as $-\varepsilon f'(\theta)\hat{\mathbf{r}} + V\hat{\mathbf{z}}$. Looking in the

frame moving with speed V, we observe a force-free surface that does not swim and has a boundary condition $-\varepsilon f'(\theta)\hat{\mathbf{r}}$ (a Galilean transformation does not vary the force on the body). This observed surface is exactly that under consideration and thus internal helical wave pumping is force-free for a non-rotating surface for any boundary geometry (at any amplitude).

The axial component of the flow internal to the body is found by carrying out a similar calculation as in Sec. III A. Once again, the entire flow field must be determined at $O(\varepsilon)$. Using the same method and notation as in the external flow calculation, the $k \neq 0$ modes of the pressure and axial velocity field at $O(\varepsilon)$ are given by

$$\mathscr{P}_k = -ikC_q I_q(\lambda), \tag{51}$$

$$\mathscr{W}_k = \frac{C_q}{2\nu}\left(\frac{q\nu I_{q-1}(q\nu)}{I_q(q\nu)} I_q(\lambda) - \lambda I_{q-1}(\lambda)\right), \tag{52}$$

where $q = |k|$ and $\lambda = q\nu r$, but now we have retained only the modified Bessel functions that are finite at the origin. In the above, we have

$$C_q = \frac{2\left(-q + \dfrac{q\nu I_{q-1}}{I_q}\right)}{-qI_q + q\nu I_{q-1} + \dfrac{2(2-q)}{\nu} I_{q-1} + \dfrac{(3q-2)I_{q-1}^2}{I_q} - \dfrac{q\nu I_{q-1}^3}{I_q^2}}, \tag{53}$$

where $I_{q-1} = I_{q-1}(q\nu)$ and $I_q = I_q(q\nu)$. Then, using the boundary condition, $w_2(1,\theta) = -f(\theta)\partial w_1(1,\theta)/\partial r$, the $k = 0$ mode of the axial pumping flow is found to be

$$\hat{w}_{20} = -2\sum_{q\geq 1} |\hat{f}_q|^2 H_q, \tag{54}$$

where

$$H_q = \frac{d\mathscr{W}_q}{dr}(1) = \frac{q^2 C_q}{2}\left(-2I_{q-1} - \nu I_q + \nu\frac{I_{q-1}^2}{I_q}\right) > 0, \tag{55}$$

and therefore, the leading order expression for the internal pumping flow is given by

$$R(\varepsilon) = 2\pi\varepsilon^2 \sum_{q\geq 1} |\hat{f}_q|^2 H_q. \tag{56}$$

The fluid pumping is always in the direction of wave motion (in the direction of $-\hat{\mathbf{z}}$), just as is the case for transverse wave propagation for the case of the infinite sheet.[20] Figure 7 shows the scaled pumping rate, R/ε^2, as a function of ν. We see that the $O(\varepsilon^2)$ theory is quite good for a wide range of ν but deteriorates in accuracy as the helical pitch is decreased (increasing ν). The pumping rate increases with ν in apparently monotonic growth.

Meanwhile, the in-plane components of the velocity field for internal flow are given by

$$\mathscr{U}_k = ikD_q\frac{I_q(\lambda)}{\lambda} + \frac{ikC_q}{2q\nu}\left(-\lambda I_q(\lambda) + \left(2 - q + \frac{q\nu I_{q-1}(q\nu)}{I_q(q\nu)}\right) I_{q-1}(\lambda)\right), \tag{57}$$

$$\mathscr{V}_k = \frac{1}{q}\lambda\mathscr{W}_k - \frac{1}{ik}\frac{d}{d\lambda}(\lambda\mathscr{U}_k), \tag{58}$$

where

$$D_q = -\frac{q\nu}{I_q(q\nu)} - \frac{C_q}{2I_q(q\nu)}\left(-q\nu I_q(q\nu) + \left(2 - q + \frac{q\nu I_{q-1}(q\nu)}{I_q(q\nu)}\right) I_{q-1}(q\nu)\right). \tag{59}$$

For instance, for a single-mode helical wave with $f(\theta) = \cos(N\theta)$, the velocity field is given by

$$\mathbf{u} = \varepsilon\left(\cos(N\theta)(\mathscr{V}_N\hat{\boldsymbol{\theta}} + \mathscr{W}_N\hat{\mathbf{z}}) + i\sin(N\theta)\mathscr{U}_N\hat{\mathbf{r}}\right) + O(\varepsilon^2), \tag{60}$$

where $\theta = \varphi - \nu\zeta - t$.

The analytical velocity fields at $O(\varepsilon)$ from Eq. (60) are shown in Fig. 8 for $N = 1,2,4$, and 10, with $\nu = 1$ fixed, on the domain $r \leq 1 + \varepsilon f(\theta)$. Color indicates the axial (out-of-plane) fluid

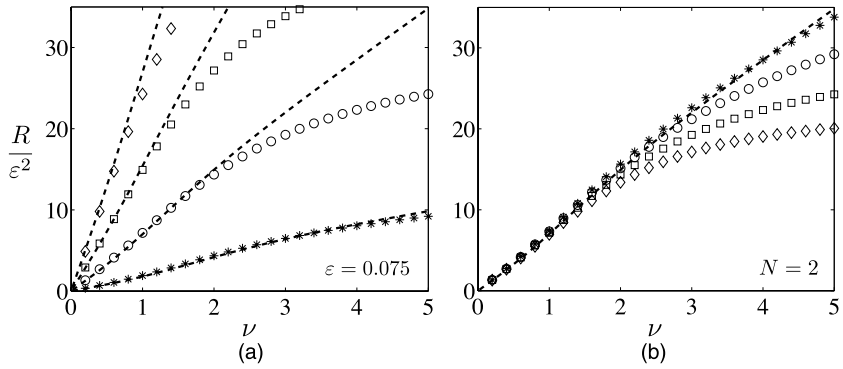

FIG. 7. The scaled pumping rate R/ε^2 as a function of ν, with R the mean flow in the $-\hat{\mathbf{z}}$ direction. (a) Pumping rate for $N = 1$ (stars), 2 (circles), 3 (squares), and 4 (diamonds), with $\varepsilon = 0.075$ fixed. Dashed lines show the predictions of the $O(\varepsilon^2)$ theory. (b) Pumping rate with $N = 2$ fixed for $\varepsilon = 0.025$ (stars), 0.05 (circles), 0.075 (squares), and 0.1 (diamonds).

velocity, while arrows indicate the in-plane fluid velocity. Since the boundary conditions for the $O(\varepsilon)$ solutions are imposed at $r = 1$ instead of at $r = 1 + \varepsilon f(\theta)$, the field does not strictly match the boundary conditions on the real boundary surface. For the $N = 1$ boundary, the flow is roughly uniform in a given cross-sectional plane near the center of the domain. For modes with $N \geq 2$, both the horizontal and axial components of the fluid flow vanish at $r = 0$ and the quiet region of small fluid velocity grows toward the boundary as N increases. For large N, the magnitude of the velocity at the surface increases in proportion to N, but the velocity field decreases to zero rapidly towards the center of the fluid domain. As Eq. (60) shows, the field depends on $\lambda = N\nu r$ which suggests the typical dimensionless length scale of the flow is $O((N\nu)^{-1})$, indicating that a boundary layer also develops in the interior flow problem. The focusing of the flow towards the boundary for increasing N, for instance, is clearly visible in Fig. 8.

For a given wave number N, the axial flow structure takes the shape of $2N$ helical fluid structures of alternating flow direction. This is shown in Fig. 8, where level sets of the instantaneous axial component of the velocity field are shown at the values $\pm\|w\|_\infty/2$ for $N = 1, 4$, and 10. Here, again it is clear that the dominant fluid flow moves towards the boundary for increased wavenumber N. The downward pumping is not at all obvious from the flow field, which includes a large reverse flow opposite the direction of mean flow. The fluid structure should not be misconstrued—as the

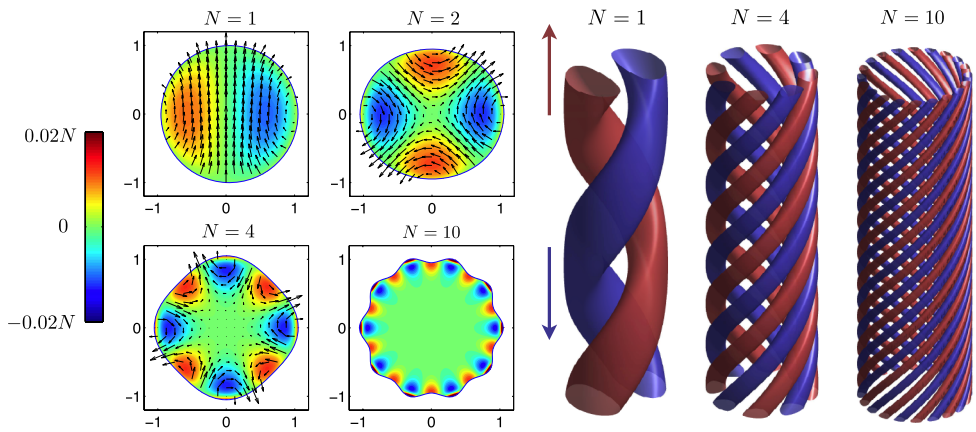

FIG. 8. The instantaneous velocity fields at $O(\varepsilon)$ (analytical values) are shown with $\nu = 1$ and $\varepsilon = 0.05$ fixed. Left: color indicates the axial (out-of-plane) fluid velocity for the same ν and ε as on the left, while arrows indicate the in-plane fluid velocity. Boundaries described by larger wavenumbers generate fluid motion nearer to the boundary and do not much disturb the central fluid region. Right: level sets of the instantaneous axial component of the velocity field are shown at the values $\pm\|w\|_\infty/2$.

helical wave passes and the helical structure shown rotates in time, Lagrangian tracer particles will observe a complicated time-dependent flow. In other words, the instantaneous helical geometry of the flow does not suggest that particles move along helical trajectories up or down through the body, and instead there are likely to be very interesting mixing dynamics throughout the domain.[67,68]

To investigate the flow structure near the center of the fluid domain, we examine the leading term of the Taylor series expansion of $I_q(\lambda) \sim \lambda^q/(2^q q!) = (q\nu r)^q/(2^q q!)$ for small λ (i.e., small r). The velocity field for $r \sim 0$ is given approximately by

$$\mathbf{u} \sim \varepsilon\left(\chi_1 r^{N-1}\left(\sin(N\theta)\hat{\mathbf{r}} + \cos(N\theta)\hat{\boldsymbol{\theta}}\right) + \chi_2 r^N \cos(N\theta)\hat{\mathbf{z}}\right), \tag{61}$$

where χ_1 and χ_2 are constants that depend on N and ν which decay exponentially fast as $N\nu \to \infty$. Just as the higher wavenumber leads to faster decay in the far-field away from an infinite swimming sheet, here we see the same effect in a circular arrangement in the internal flow. From Eq. (61), in addition to the flow vanishing at the center of the domain, we also see that the in-plane velocity dominates the axial/pumping component of the flow for all N as $r \to 0$.

V. SWIMMING AND PUMPING OF VISCOELASTIC FLUIDS

Finally, the approach taken in this paper may be applied to the study of more complex fluid flows. We conclude with the development of analytical solutions for confined/unconfined swimming and internal pumping by helical waves in viscoelastic fluids, which we model by the Stokes/Oldroyd-B equations. The dimensionless equations describing an Oldroyd-B model fluid in the viscous (Stokes) limit (see Refs. 69 and 70) are

$$-\nabla p + \nabla\cdot\boldsymbol{\tau} = \mathbf{0}, \quad \nabla\cdot\mathbf{u} = 0, \tag{62}$$

$$\boldsymbol{\tau} + \mathrm{De}\,\overset{\triangledown}{\boldsymbol{\tau}} = \dot{\boldsymbol{\gamma}} + \beta\,\mathrm{De}\,\overset{\triangledown}{\dot{\boldsymbol{\gamma}}}, \tag{63}$$

where $\dot{\boldsymbol{\gamma}} = \nabla\mathbf{u} + \nabla\mathbf{u}^T$ is the rate-of-strain tensor, $\mathrm{De} = \lambda\omega$ is the Deborah number, a ratio of the fluid relaxation timescale λ to the timescale of helical wave motion, and $\beta = \eta_s/\eta$ is the ratio of solvent viscosity to the total (solvent plus polymer) viscosity. In Eq. (63), we have introduced the upper-convected time-derivative

$$\overset{\triangledown}{\boldsymbol{\tau}} = \frac{\partial\boldsymbol{\tau}}{\partial t} + \mathbf{u}\cdot\nabla\mathbf{u} - \boldsymbol{\tau}\cdot\nabla\mathbf{u} - \nabla\mathbf{u}^T\cdot\boldsymbol{\tau}, \tag{64}$$

a time-derivative that ensures that the constitutive law, Eq. (63), is frame-invariant.[69,70]

Swimming in viscoelastic fluids by the passage of small-amplitude helical waves was considered previously by Fu *et al.*,[50] who considered an undulating thin cylinder in an infinite Oldroyd-B model fluid, and found that the swimming speed, U, compared to the swimming speed in a Newtonian fluid of the same total viscosity, U_N, satisfied

$$\frac{U}{U_N} = \frac{1+\beta\,\mathrm{De}^2}{1+\mathrm{De}^2}, \tag{65}$$

at $O(\varepsilon^2)$ for near-cylinders, which matched the same ratio found previously for infinite swimming sheets by Lauga[71] and for planar undulating filaments by Fu *et al.*[72] The swimming speed is therefore always smaller than that in a Newtonian fluid for small amplitude sinusoidal undulations. However, at larger helical amplitudes, fluid elasticity can actually enhance the swimming speed, as was shown in experiments by Liu *et al.*[73] and numerically by Spagnolie *et al.*[51]

To find the asymptotic solution to Eqs. (62) and (63) for small amplitude waves, we perform the same regular perturbation expansion as in Eq. (22). The deviatoric stress tensor $\boldsymbol{\tau}$ is now similarly written as a regular expansion in powers of ε. Recall the boundary condition for the external swimming problem,

$$\mathbf{u}(\mathbf{x}\in\partial S) = -\varepsilon f'(\theta)\hat{\mathbf{r}} + \Omega(1+\varepsilon f(\theta))\hat{\boldsymbol{\theta}} + U\hat{\mathbf{z}}. \tag{66}$$

Unfortunately, we may no longer use the linearity of the Stokes equations to decompose the problem into helical wave and a compensating rigid body rotation to find the rotation rate Ω. Instead, we

will proceed leaving the full boundary conditions intact. Following Spagnolie *et al.*,[51] once the body and fluid have reached a quasi-steady state, we have

$$\frac{\partial}{\partial t} = \left(\frac{1+\Omega}{\nu} - U\right)\frac{\partial}{\partial z} = \left(\frac{1+\Omega}{\nu} - U\right)\left(\frac{\partial}{\partial \zeta} - \nu\frac{\partial}{\partial \theta}\right). \tag{67}$$

In a frame moving with velocity $[U - (1+\Omega)\nu^{-1}]\hat{\mathbf{z}}$, setting $\tilde{z} = z - [U - (1+\Omega)\nu^{-1}]t$, the observed fluid field is steady since the boundary and boundary conditions are steady. Physical quantities then take the form $\Phi(x, y, \tilde{z})$, from which we see $\partial_t \Phi|_{x,y,z} = [(1+\Omega)\nu^{-1} - U]\partial_z \Phi|_{x,y,t}$. Then recalling the relation $\partial_z = \partial_\zeta - \nu\partial_\theta$, we recover the expression above.

Clearly $U = 0$ and $\Omega = 0$ when $\varepsilon = 0$. Assuming $\Omega(\varepsilon)$ is regular around $\varepsilon = 0$, the constitutive equation at $O(\varepsilon)$ is given by

$$\boldsymbol{\tau}_1 + \frac{\mathrm{De}}{\nu}\left(\frac{\partial}{\partial \zeta} - \nu\frac{\partial}{\partial \theta}\right)\boldsymbol{\tau}_1 = \dot{\boldsymbol{\gamma}}_1 + \frac{\beta\,\mathrm{De}}{\nu}\left(\frac{\partial}{\partial \zeta} - \nu\frac{\partial}{\partial \theta}\right)\dot{\boldsymbol{\gamma}}_1. \tag{68}$$

To proceed, we adopt the Fourier decomposition of $f(\theta)$ as before. For notational convenience, we define

$$\mathbf{u}_{1k} = \hat{u}_{1k}\hat{\mathbf{r}} + \hat{v}_{1k}\hat{\boldsymbol{\theta}} + \hat{w}_{1k}\hat{\mathbf{z}}, \tag{69}$$

the kth Fourier coefficient of each component being $\hat{u}_{1k}$, etc., so that we can write $\mathbf{u}_1 = \sum_k \mathbf{u}_{1k} \exp(ik\theta)$. Note that the vector coefficients $\mathbf{u}_{1k}$ are not the Fourier coefficients of the vector $\mathbf{u}_1$ due to the dependence of the basis vectors on θ. Similarly, and again for convenience, let $\mathbf{e}_i \in \{\hat{\mathbf{r}}, \hat{\boldsymbol{\theta}}, \hat{\mathbf{z}}\}$ and suppose the (i, j) component of a tensor $\boldsymbol{\tau}_1$ is $\tau_{1,ij}$, the kth Fourier coefficient being $\hat{\tau}_{1,ij,k}$. We define

$$\boldsymbol{\tau}_1^{(k)} = \sum_{i,j} \hat{\tau}_{1,ij,k}\mathbf{e}_i\mathbf{e}_j, \tag{70}$$

so that we may write $\boldsymbol{\tau}_1 = \sum_k \boldsymbol{\tau}_1^{(k)} e^{ik\theta}$. Again, due to the θ dependence of the basis vectors, $\boldsymbol{\tau}_1^{(k)}$ is not a tensor Fourier transform of $\boldsymbol{\tau}_1$. However, the benefit of the notational choices above is that the rate-of-strain tensor now satisfies the simple relation

$$\dot{\boldsymbol{\gamma}}_1^{(k)} \exp(ik\theta) = \nabla(\mathbf{u}_{1k}\exp(ik\theta)) + \nabla(\mathbf{u}_{1k}\exp(ik\theta))^T, \tag{71}$$

where $\dot{\boldsymbol{\gamma}}_1 = \sum_k \dot{\boldsymbol{\gamma}}_1^{(k)} \exp(ik\theta)$. Upon insertion of the above into the constitutive equation, we obtain

$$\boldsymbol{\tau}_1^{(k)} = \eta^*(k)\dot{\boldsymbol{\gamma}}_1^{(k)}, \tag{72}$$

which is very similar to the Fourier transform of the Newtonian constitutive law, but with a mode-dependent *complex viscosity*, $\eta^*(k) = (1 - ik\beta\,\mathrm{De})/(1 - ik\,\mathrm{De})$ (see Ref. 69). The real part of the complex viscosity governs the dissipation of energy in the fluid, while the imaginary part of the complex viscosity governs the stored elastic energy during deformation. From Eq. (62), we have

$$\nabla(\hat{p}_{1k}\exp(ik\theta)) = \eta^*(k)\nabla^2(\mathbf{u}_{1k}\exp(ik\theta)). \tag{73}$$

Introducing the effective pressure $\hat{p}_{1k} = \eta^*(k)\tilde{p}_k$, we recover exactly the same equations at $O(\varepsilon)$ as in the Stokes flows studied in Secs. III and IV. With the same force-free condition, we see that the $O(\varepsilon)$ velocity field is the same as that in Stokes flow, namely, we have $\mathbf{u}_{1k} = (\mathcal{U}_k\hat{\mathbf{r}} + \mathcal{V}_k\hat{\boldsymbol{\theta}} + \mathcal{W}_k\hat{\mathbf{z}})\hat{f}_k$ and then $U_1 = 0$ and $U = O(\varepsilon^2)$. Furthermore, the torque for each mode at $O(\varepsilon)$ is zero by the results in Stokes flow. This shows that the torque contributed by the helical wave still enters as $O(\varepsilon^2)$ in the Oldroyd-B fluid as does the rigid body rotation rate Ω. We will consider the swimming speed and pumping rate to $O(\varepsilon^2)$ only, so that we may neglect the rigid body rotation in the viscoelastic case.

The swimming speed or pumping rate at $O(\varepsilon^2)$ is again only related to the $k = 0$ mode. The $k = 0$ mode of the constitutive equation at $O(\varepsilon^2)$ reads

$$\begin{aligned}\boldsymbol{\tau}_2^{(0)} + \mathrm{De}\Big((\mathbf{u}_1\cdot\nabla\boldsymbol{\tau}_1)^{(0)} - (\boldsymbol{\tau}_1\cdot\nabla\mathbf{u}_1 + \nabla\mathbf{u}_1^T\cdot\boldsymbol{\tau}_1)^{(0)}\Big)\\ = \dot{\boldsymbol{\gamma}}_2^{(0)} + \beta\,\mathrm{De}\Big((\mathbf{u}_1\cdot\nabla\dot{\boldsymbol{\gamma}}_1)^{(0)} - (\dot{\boldsymbol{\gamma}}_1\cdot\nabla\mathbf{u}_1 + \nabla\mathbf{u}_1^T\cdot\dot{\boldsymbol{\gamma}}_1)^{(0)}\Big),\end{aligned} \tag{74}$$

as the $\partial/\partial t$ derivative from (67) on the "(0)" quantities above is zero. Equations (62) for $k = 0$ read (noticing that $\tau^{(0)}_{2,rr} = \hat{\tau}_{2,rr,0}$)

$$\hat{\mathbf{r}}\frac{d\hat{p}_{20}}{dr} = \left(\frac{d}{dr}\tau^{(0)}_{2,rr} + \frac{\tau^{(0)}_{2,rr}}{r} - \frac{\tau^{(0)}_{2,\theta\theta}}{r}\right)\hat{\mathbf{r}} + \left(\frac{d}{dr}\tau^{(0)}_{2,r\theta} + \frac{2\tau^{(0)}_{2,r\theta}}{r}\right)\hat{\boldsymbol{\theta}} + \left(\frac{d}{dr}\tau^{(0)}_{2,rz} + \frac{\tau^{(0)}_{2,rz}}{r}\right)\hat{\mathbf{z}}, \tag{75}$$

$$\frac{d\hat{u}_{2,0}}{dr} + \frac{\hat{u}_{2,0}}{r} = 0. \tag{76}$$

Upon inspection of the above, we see that

$$\hat{u}_{2,0} \propto \frac{1}{r}, \quad \tau^{(0)}_{2,rz} \propto \frac{1}{r}, \quad \tau^{(0)}_{2,r\theta} \propto \frac{1}{r^2}. \tag{77}$$

Recalling that the boundary condition on w contains the swimming speed at second order (see Eq. (24)), we once again are tasked with determining $\hat{w}_{20}(1)$. This quantity appears in the rz component of the constitutive equation, Eq. (74),

$$\tau^{(0)}_{2,rz} - \frac{d}{dr}\hat{w}_{20} = -\alpha_{rz} + \kappa_{rz} + \kappa_{zr}, \tag{78}$$

where $\boldsymbol{\alpha} = \mathrm{De}\left(\mathbf{u}_1 \cdot \nabla(\boldsymbol{\tau}_1 - \beta\dot{\boldsymbol{\gamma}}_1)\right)^{(0)}$ and $\boldsymbol{\kappa} = \mathrm{De}\left((\boldsymbol{\tau}_1 - \beta\dot{\boldsymbol{\gamma}}_1)\cdot\nabla\mathbf{u}_1\right)^{(0)}$. Given that we must have $\mathcal{U}_{-k} = -\mathcal{U}_k$, $\mathcal{V}_{-k} = \mathcal{V}_k$, and $\mathcal{W}_{-k} = \mathcal{W}_k$, and after a tedious computation we find

$$\kappa_{rz} + \kappa_{zr} - \alpha_{rz} = \sum_k \frac{(1-\beta)\mathrm{De}\,|\hat{f}_k|^2}{1 - ik\,\mathrm{De}}\left(\frac{d}{dr}\frac{1}{r}\frac{d}{dr}(\mathcal{W}_{-k}r\mathcal{U}_k)\right). \tag{79}$$

Using this expression, we find that $\tau^{(0)}_{2,rz}$ must be zero for all cases, though the arguments for the different cases differ slightly. Integrating Eq. (78), we finally obtain the swimming speed up to $O(\varepsilon^2)$,

$$U = 2\varepsilon^2 \sum_{q\geq 1} \frac{(1+\beta q^2\mathrm{De}^2)|\hat{f}_q|^2}{1+q^2\mathrm{De}^2} J_q = 2\varepsilon^2 \sum_{q\geq 1} \Re[\eta^*(q)]|\hat{f}_q|^2 J_q, \tag{80}$$

where $\Re[z]$ is the real part of z, and J_q is given in Eq. (35) for confined swimming and more directly in Eq. (36) for unconfined swimming. The result above shows that the real part of the complex viscosity is the primary quantity that sets the swimming speed of helical bodies of arbitrary (small-amplitude) cross-sectional profile, even for confined swimming inside a cylindrical tube. The $L \to \infty$ limit matches the result by Fu *et al.* for a single Fourier mode boundary geometry.[50]

The relationship between the complex viscosity and locomotion by traveling waves is quite interesting, as quadratic terms, $O(\varepsilon^2)$, are necessary to understand locomotion (see Ref. 71), but the complex viscosity is due to the linear, $O(\varepsilon)$, flow field. This issue is considered in detail by Elfring and Lauga[37] for swimming sheets of arbitrary shape and undulation frequency in both an infinite and a wall-bounded fluid domain, who found the same pre-factor as in the above in the swimming problem, and by Lauga,[74] who discusses a much larger class of swimming bodies and complex fluids. A related variation was found in the synchronization of two infinite sheets by Elfring *et al.*[75]

A similar calculation returns the rate of fluid pumping in the internal problem

$$\hat{w}_{20}(r) = -\sum_k \frac{(1+\beta q^2\mathrm{De}^2)|\hat{f}_k|^2}{1+q^2\mathrm{De}^2} H_q - \sum_k \frac{(1-\beta)\mathrm{De}^2|\hat{f}_k|^2}{1+q^2\mathrm{De}^2}\left(\frac{ik}{r}\frac{d}{dr}(\mathcal{W}_{-k}r\mathcal{U}_k)\right), \tag{81}$$

where the flow fields are now those from the internal pumping problem in Sec. IV. If we consider the pumping rate by the surface in the $-\hat{\mathbf{z}}$ direction, we have at $O(\varepsilon^2)$ that

$$\begin{aligned} R(\varepsilon) &= -2\pi\varepsilon^2 \int_0^1 r\,\hat{w}_{20}(r)\,dr \\ &= 2\pi\varepsilon^2 \sum_{q\geq 1} \frac{(1+\beta q^2\mathrm{De}^2)|\hat{f}_q|^2}{1+q^2\mathrm{De}^2} H_q = 2\pi\varepsilon^2 \sum_{q\geq 1} \Re[\eta^*(q)]|\hat{f}_q|^2 H_q. \end{aligned} \tag{82}$$

So in fact, the adjustment of the Newtonian fluid flow in the internal pumping problem at $O(\varepsilon^2)$ is also directly related to the complex viscosity.

VI. DISCUSSION

In this paper, we used a helical coordinate system to derive closed-form analytical expressions for the swimming and pumping of helical bodies by the propagation of helical waves in viscous and viscoelastic fluids. A Fourier analysis in the small wave amplitude limit was used so that exact expressions at second order, $O(\varepsilon^2)$, were obtained for all problems studied. In the external flow problem of force- and torque-free swimming, we found the torque-balancing rigid body rotation rate and the swimming speed of the cylinder were computed to $O(\varepsilon^4)$ using matched asymptotics for single-mode helical waves. The introduction of a confining cylindrical tube was found to significantly enhance the swimming speed, and the complicated dependence upon the helical pitch showed multiple extrema. The effect of confinement, however, was found to diminish exponentially fast with the radius of the outer cylindrical tube. Similar results were found for the internal Stokes flow problem and the exact pumping rate at $O(\varepsilon^2)$ was calculated. Finally, we recovered the confined/unconfined swimming speed and internal pumping rate in a viscoelastic (Oldroyd-B) fluid for helical bodies of arbitrary cross section, which all depended upon the real part of the complex viscosity. Although the swimming speeds were only given explicitly in the unconfined case, the limiting values as $L \to \infty$ were identical to the results for infinite swimming (setting $L = \infty$); that the limit is not singular is consistent with the decay of the far-field fluid flow in force-free locomotion.[1]

The swimming speeds, rotation rates, and pumping rates derived in this work may be useful in understanding the hydrodynamics of swimming microorganisms, including the helical-wave swimming of *Synechococcus*,[16] or in the effort to design helical synthetic microswimmers.[76–81] Consider for instance a typical *Paramecium*. Taking values from Refs. 3, 4, and 18, the body length is roughly 200 μm, the width is $2A \approx 50$ μm, and the beating angle $\beta \approx 70°$ corresponds to $\nu = \tan(\beta) = 2.7$. The metachronal wavelength is approximately $2\pi A \sin\beta/(N\nu) \approx 10$ μm, so that the cross-sectional wavenumber is estimated to be $N \approx 2\pi A \sin(7\pi/18)/(\tan\beta\lambda) \approx 5$. The measured cilium length is approximately 10 μm, and taking half this value to model the helical wave amplitude, we set $\varepsilon \sim 5/25 = 0.2$. Using the $O(\epsilon^2)$ theory, we would estimate a scaled swimming speed of $U \approx 31$. Then with the beat frequency given approximately by $\omega = 2\pi f = 2\pi * 28$ Hz, the dimensional speed is estimated to be $\varepsilon^2\omega AU = 5400$ μm/s. The actual swimming speed of *Paramecium* is closer to $800 - 1200$ μm/s. The theory overestimates the swimming speed but is on the same order of magnitude. The body in Fig. 1(a) is clearly not cylindrical, or infinite, but note also that the swimming speed is very sensitive to ε and a smaller value of ε may be appropriate for modeling the effective ciliary wave amplitude (see Fig. 1(c)). The discrepancy may also be related to the absence of a ciliary recovery stroke in the present model. Other applications and limitations of the envelope model of ciliary propulsion were discussed in detail by Blake and Sleigh.[3]

In the case of confined swimming, unlike the increase in swimming speed due to confinement found in the present study, Jana *et al.*[10] observed experimentally that the swimming speed of *Paramecium* actually decreases with confinement. The discrepancy points to an experimentally well-established fact: the rate of ciliary actuation is dependent upon fluid stresses and other properties, and ciliary beat frequency (and hence the wave speed in the swimming of a confined *Paramecium*) decreases with increased resistance.[18]

Future work may include optimization of swimming and pumping by helical waves in the present contexts and an analysis of mixing by the flow fields produced in the internal pumping problem. The time-dependence of the flow as numerous counter-flowing fluid helices rotate about the central axis is likely to lead to rapid departures of neighboring particles and positive Lyapunov exponents, the hallmark of chaotic fluid mixing.[67] Such internal helical flows have been observed in cytoplasmic streaming in such large eukaryotic cells as the alga *Chara corallina* (albeit by a different boundary velocity than the helical waves studied here), and it has been suggested by Goldstein *et al.* that the

associated mixing may be important in nutrient distribution in internal biological flows.[68] The ubiquity of the complex viscosity in swimming and pumping here and in related problems in viscoelastic fluids is an ongoing topic of research.[37]

ACKNOWLEDGMENTS

We are grateful to Gwynn Elfring for helpful comments.

APPENDIX A: THE IN-PLANE VELOCITY FIELD IN THE EXTERNAL SWIMMING PROBLEM

Performing a similar analysis as was done for rigid body motion in Ref. 59, the first of the in-plane components of the velocity field in the external swimming problem for a general container size L is found to be

$$\mathcal{U}_k = -\frac{ika_q}{2q\nu}\lambda K_q - \frac{ikb_q}{2q\nu}\lambda I_q - \frac{ik}{2}\left(\frac{2a_q}{q\nu} - \frac{a_q}{\nu} + \frac{2c_q}{q}\right)K_{q-1} + \frac{ik}{2}\left(\frac{2b_q}{q\nu} - \frac{b_q}{\nu} + \frac{2d_q}{q}\right)I_{q-1} + \frac{ik\xi_q}{\lambda}K_q + \frac{ik\tilde{\xi}_q}{\lambda}I_q, \quad \text{(A1)}$$

where $q = |k|$, and ξ_q and $\tilde{\xi}_q$ are two new unknown coefficients that are set by the boundary conditions in Eq. (30), as described in Sec. III. In the case $L \to \infty$, we have

$$\mathcal{U}_k = -ik\frac{A_q}{q\nu}\left(\frac{1}{2}\lambda K_q(\lambda) - \frac{1}{2}\left(q - 2 + \frac{q\nu K_{q-1}(q\nu)}{K_q(q\nu)}\right)K_{q-1}(\lambda)\right) + ikB_q\frac{K_q(\lambda)}{\lambda}, \quad \text{(A2)}$$

where

$$B_q = \frac{A_q\left(q\nu K_q - \left(q - 2 + \frac{q\nu K_{q-1}}{K_q}\right)K_{q-1}\right) - 2q\nu}{2K_q(q\nu)}. \quad \text{(A3)}$$

The incompressibility condition then may be used to deduce the second component of the in-plane velocity field,

$$\mathcal{V}_k = \frac{1}{q}\lambda\mathcal{W}_k - \frac{1}{ik}\frac{d}{d\lambda}(\lambda\mathcal{U}_k). \quad \text{(A4)}$$

APPENDIX B: HYDRODYNAMIC FORCE AND TORQUE PER UNIT LENGTH

The hydrodynamic force per unit length on the helical body is found by integrating the fluid stress around a cross section. The surface element is $d\mathbf{S} = (\mathbf{x}^S)_\theta \times (\mathbf{x}^S)_\zeta\, d\theta d\zeta = \mathbf{n}\, d\theta d\zeta$, with $\mathbf{n}$ an unnormalized normal vector at the boundary surface (see Eq. (1)). We have that

$$\mathcal{F} = \hat{\mathbf{z}} \cdot \int_0^{2\pi} \boldsymbol{\sigma} \cdot \mathbf{n}\big|_{\zeta=0}\, d\theta = \int_0^{2\pi}\left\{-\nu\rho\rho' p + \rho\left(\frac{\partial w}{\partial r} - \nu\frac{\partial u}{\partial\theta}\right) - \rho'\left(\frac{1}{\rho}\frac{\partial w}{\partial\theta} - \nu\frac{\partial v}{\partial\theta}\right) - 2\nu^2\rho\rho'\frac{\partial w}{\partial\theta}\right\}d\theta. \quad \text{(B1)}$$

Recalling that $\rho(\theta) = 1 + \varepsilon f(\theta)$, expanding about $\rho = 1$, and keeping terms to $O(\varepsilon^2)$, the force per unit length may be written as

$$\mathcal{F} = \varepsilon\int\left(\frac{\partial w_1}{\partial r} - \nu\frac{\partial u_1}{\partial\theta}\right)_{r=1} d\theta + \varepsilon^2\int\left(\frac{\partial w_2}{\partial r} - \nu\frac{\partial u_2}{\partial\theta}\right)_{r=1} d\theta + \varepsilon^2\int\left\{-\nu p_1 f'(\theta) + f(\theta)\left(\frac{\partial w_1}{\partial r} - \nu\frac{\partial u_1}{\partial\theta} + \frac{\partial^2 w_1}{\partial r^2} - \nu\frac{\partial^2 u_1}{\partial r\partial\theta}\right) - f'(\theta)\left(\frac{\partial w_1}{\partial\theta} - \nu\frac{\partial v_1}{\partial\theta}\right) - 2\nu^2 f'(\theta)\frac{\partial w_1}{\partial\theta}\right\}\Big|_{r=1} d\theta. \quad \text{(B2)}$$

The first integral is zero for the helical wave problem, and the second evaluates to $2\pi\varepsilon^2\hat{w}'_{20}(1)$. The third integral, denoted as $\mathscr{F}_3$, can be written as

$$\mathscr{F}_3 = 2\pi\varepsilon^2 \sum_k |\hat{f}_k|^2 \left\{ ik\nu\mathscr{P}_k + \mathscr{W}'_k - ik\nu\mathscr{U}_k + \mathscr{W}''_k - \nu ik\mathscr{U}'_k - k^2\mathscr{W}_k + \nu k^2\mathscr{V}_k - 2\nu^2 k^2\mathscr{W}_k \right\}. \tag{B3}$$

However, using Eq. (19), the expression in the curly braces above reduces to

$$(-ik\nu\mathscr{U}_k - \nu ik\mathscr{U}'_k + \nu k^2\mathscr{V}_k - \nu^2 k^2\mathscr{W}_k)_{r=1},$$

which is zero by the incompressibility condition, Eq. (20). So in fact, the axial force per unit length on the helical body due to the passage of helical waves, accurate up to $O(\varepsilon^2)$, is simply

$$\mathscr{F} = 2\pi\varepsilon^2\hat{w}'_{20}(1). \tag{B4}$$

The torque per unit length on the helical body is calculated similarly,

$$\begin{aligned}\mathscr{L} &= \hat{\mathbf{z}} \cdot \int_0^{2\pi} \mathbf{x}^S \times (\boldsymbol{\sigma} \cdot \mathbf{n})\Big|_{\zeta=0} d\theta \\ &= \int_0^{2\pi} \left\{ \rho\rho' p + \left(-\rho v + \rho^2 \frac{\partial v}{\partial r}\right) + \rho\frac{\partial u}{\partial \theta} - 2\rho'\left(\frac{\partial v}{\partial \theta} + u\right) + \nu\rho\rho'\left(\frac{\partial w}{\partial \theta} - \nu\rho\frac{\partial v}{\partial \theta}\right)\right\} d\theta. \end{aligned} \tag{B5}$$

Expanding about $\rho = 1$ and working to $O(\varepsilon^2)$, the expression reduces to

$$\begin{aligned}\mathscr{L} = \varepsilon \int_0^{2\pi} \left(\frac{\partial v_1}{\partial r} - v_1\right)_{r=1} d\theta + \varepsilon^2 \int_0^{2\pi} \left(\frac{\partial v_2}{\partial r} - v_2\right)_{r=1} d\theta + \int_0^{2\pi} \left(\varepsilon\frac{\partial u_1}{\partial \theta} + \varepsilon^2\frac{\partial u_2}{\partial \theta}\right)_{r=1} d\theta \\ + \varepsilon^2 \int_0^{2\pi} \Big\{ f'(\theta)p_1 + \left(-v_1 + \frac{\partial v_1}{\partial r} + \frac{\partial^2 v_1}{\partial r^2}\right) f(\theta) + f(\theta)\frac{\partial u_1}{\partial \theta} + f(\theta)\frac{\partial^2 u_1}{\partial r \partial \theta} \\ - 2f'(\theta)u_1 + \nu f'(\theta)\frac{\partial w_1}{\partial \theta} - (2+\nu^2) f'(\theta)\frac{\partial v_1}{\partial \theta}\Big\}_{r=1} d\theta + O(\varepsilon^3). \end{aligned} \tag{B6}$$

The first and the third integrals are zero using the boundary conditions in the helical wave problem, and the second integral evaluates to $2\pi\varepsilon^2\left(\hat{v}'_{20}(1) - \hat{v}_{20}(1)\right)$. The last integral, denoted as $\mathscr{L}_4$, may be written as

$$\begin{aligned}\mathscr{L}_4 = 2\pi\varepsilon^2 \sum_k |\hat{f}_k|^2 \Big\{ -ik\mathscr{P}_k + \left(-\mathscr{V}_k + \mathscr{V}'_k + \mathscr{V}''_k\right) + 3ik\mathscr{U}_k + ik\mathscr{U}'_k \\ + \nu k^2\mathscr{W}_k - (2+\nu^2)k^2\mathscr{V}_k \Big\}\Big|_{r=1}. \end{aligned} \tag{B7}$$

Using Eq. (18), the expression in the curly braces above reduces to

$$\left(ik\mathscr{U}_k + ik\mathscr{U}'_k + \nu k^2\mathscr{W}_k - k^2\mathscr{V}_k\right)\Big|_{r=1},$$

which once again is zero by the incompressibility condition, Eq. (20). Therefore, $\mathscr{L}_4 = 0$ and the torque per unit length on the helical body due to the passage of helical waves, accurate up to $O(\varepsilon^2)$, is simply

$$\mathscr{L} = 2\pi\varepsilon^2\left(\hat{v}'_{20}(1) - \hat{v}_{20}(1)\right). \tag{B8}$$

[1] E. Lauga and T. R. Powers, "The hydrodynamics of swimming microorganisms," Rep. Prog. Phys. **72**, 096601 (2009).
[2] M. A. Sleigh, *Cilia and Flagella* (Academic Press, 1974).
[3] J. R. Blake and M. A. Sleigh, "Mechanics of ciliary locomotion," Biol. Rev. **49**, 85–125 (1974).
[4] C. Brennen and H. Winet, "Fluid mechanics of propulsion by cilia and flagella," Annu. Rev. Fluid Mech. **9**, 339–398 (1977).
[5] K. Drescher, K. C. Leptos, I. Tuval, T. Ishikawa, T. J. Pedley, and R. E. Goldstein, "Dancing volvox: Hydrodynamic bound states of swimming algae," Phys. Rev. Lett. **102**, 168101 (2009).
[6] C. Linnaeus, *Systema Naturae*, 10th ed. (Salvii, Holmiae, 1758), Vol. 1, p. 824.
[7] I. Jung, T. R. Powers, and J. M. Valles, Jr., "Evidence for two extremes of ciliary motor response in a single swimming microorganism," Biophys. J. **106**, 106–113 (2014).
[8] K. Fukui and H. Asai, "Spiral motion of paramecium caudatum in a small capillary glass tube," J. Eukaryotic Microbiol. **23**, 559–563 (1976).

[9] J. Männik, R. Driessen, P. Galajda, J. E. Keymer, and C. Dekker, "Bacterial growth and motility in sub-micron constrictions," Proc. Natl. Acad. Sci. U.S.A. **106**, 14861–14866 (2009).
[10] S. Jana, S. H. Um, and S. Jung, "Paramecium swimming in capillary tube," Phys. Fluids **24**, 041901 (2012).
[11] O. S. Pak, S. E. Spagnolie, and E. Lauga, "Hydrodynamics of the double-wave structure of insect spermatozoa flagella," J. R. Soc., Interface **9**, 1908–1924 (2012).
[12] J. B. Waterbury, J. M. Willey, D. G. Franks, F. W. Valois, and S. W. Watson, "A cyanobacterium capable of swimming motility," Science **230**, 74–76 (1985).
[13] K. M. Ehlers, A. D. Samuel, H. C. Berg, and R. Montgomery, "Do cyanobacteria swim using traveling surface waves?," PNAS **93**, 8340–8343 (1996).
[14] H. A. Stone and A. D. T. Samuel, "Propulsion of microorganisms by surface distortions," Phys. Rev. Lett. **77**, 4102–4104 (1996).
[15] B. Brahamsha, "Non-flagellar swimming in marine Synechococcus," J. Mol. Microbiol. Biotechnol. **1**, 59–62 (1999).
[16] K. Ehlers and G. Oster, "On the mysterious propulsion of Synechococcus," PloS One **7**, e36081 (2012).
[17] S. L. Tamm, "Ciliary motion in paramecium a scanning electron microscope study," J. Cell Biol. **55**, 250–255 (1972).
[18] H. Machemer, "Ciliary activity and the origin of metachrony in Paramecium: Effects of increased viscosity," J. Exp. Biol. **57**, 239–259 (1972).
[19] B. Nan, M. J. McBride, J. Chen, D. R. Zusman, and G. Oster, "Bacteria that glide with helical tracks," Curr. Biol. **24**, R169–R173 (2014).
[20] G. Taylor, "Analysis of the swimming of microscopic organisms," Proc. R. Soc. A **209**(1099), 447–461 (1951).
[21] M. J. Lighthill, "On the squirming motion of nearly spherical deformable bodies through liquids at very small Reynolds numbers," Commun. Pure Appl. Math. **5**, 109–118 (1952).
[22] J. R. Blake, "A spherical envelope approach to ciliary propulsion," J. Fluid Mech. **46**, 199–208 (1971).
[23] J. Blake, "Model for micro-structure in ciliated organisms," J. Fluid Mech. **55**, 1–23 (1972).
[24] C. Brennen, "An oscillating-boundary-layer theory for ciliary propulsion," J. Fluid Mech. **65**, 799–824 (1974).
[25] S. Childress, *Mechanics of Swimming and Flying* (Cambridge University Press, 1981), Vol. 2.
[26] T. Ishikawa, M. P. Simmonds, and T. J. Pedley, "Hydrodynamic interaction of two swimming model micro-organisms," J. Fluid Mech. **568**, 119–160 (2006).
[27] A. Kanevsky, M. J. Shelley, and A.-K. Tornberg, "Modeling simple locomotors in Stokes flow," J. Comput. Phys. **229**, 958–977 (2010).
[28] Y. Or and R. M. Murray, "Dynamics and stability of a class of low Reynolds number swimmers near a wall," Phys. Rev. E **79**, 045302 (2009).
[29] D. Crowdy, "Treadmilling swimmers near a no-slip wall at low Reynolds number," Int. J. Nonlinear Mech. **46**, 577–585 (2011).
[30] S. E. Spagnolie and E. Lauga, "Hydrodynamics of self-propulsion near a boundary: Predictions and accuracy of far-field approximations," J. Fluid Mech. **700**, 105–147 (2012).
[31] K. Ishimoto and E. A. Gaffney, "Squirmer dynamics near a boundary," Phys. Rev. E **88**(6), 062702 (2013).
[32] O. S. Pak and E. Lauga, "Generalized squirming motion of a sphere," J. Eng. Math. **88**, 1–28 (2014).
[33] Z. Lin, J.-L. Thiffeault, and S. Childress, "Stirring by squirmers," J. Fluid Mech. **669**, 167–177 (2011).
[34] S. Wang and A. M. Ardekani, "Unsteady swimming of small organisms," J. Fluid Mech. **702**, 286–297 (2012).
[35] L. Zhu, M. Do-Quang, E. Lauga, and L. Brandt, "Locomotion by tangential deformation in a polymeric fluid," Phys. Rev. E **83**, 011901 (2011).
[36] L. Zhu, E. Lauga, and L. Brandt, "Self-propulsion in viscoelastic fluids: Pushers vs. pullers," Phys. Fluids **24**, 051902 (2012).
[37] G. J. Elfring and E. Lauga, "Theory of locomotion through complex fluids," in *Complex Fluids in Biological Systems* (Springer, 2015), pp. 283–317.
[38] S. Michelin and E. Lauga, "Efficiency optimization and symmetry-breaking in a model of ciliary locomotion," Phys. Fluids **22**, 111901 (2010).
[39] N. Osterman and A. Vilfan, "Finding the ciliary beating pattern with optimal efficiency," Proc. Natl. Acad. Sci. U.S.A. **108**, 15727–15732 (2011).
[40] K. Ishimoto and E. A. Gaffney, "Swimming efficiency of spherical squirmers: Beyond the Lighthill theory," Phys. Rev. E **90**(1), 012704 (2014).
[41] J. Elgeti and G. Gompper, "Emergence of metachronal waves in cilia arrays," Proc. Natl. Acad. Sci. U.S.A. **110**, 4470–4475 (2013).
[42] L. Zhu, E. Lauga, and L. Brandt, "Low-Reynolds-number swimming in a capillary tube," J. Fluid Mech. **726**, 285–311 (2013).
[43] E. Setter, I. Bucher, and S. Haber, "Low-Reynolds-number swimmer utilizing surface traveling waves: Analytical and experimental study," Phys. Rev. E **85**, 066304 (2012).
[44] A. T. Chwang and T. Y. Wu, "Helical movement of micro-organisms," Proc. R. Soc. B **178**, 327–346 (1971).
[45] J. J. L. Higdon, "A hydrodynamic analysis of flagellar propulsion," J. Fluid Mech. **90**, 685–711 (1979).
[46] B. U. Felderhof, "Swimming at low Reynolds number of a cylindrical body in a circular tube," Phys. Fluids **22**, 113604 (2010).
[47] J. J. L. Higdon, "The hydrodynamics of flagellar propulsion: Helical waves," J. Fluid Mech. **94**, 331–351 (1979).
[48] N. Phan-Thien, T. Tran-Cong, and M. Ramia, "A boundary-element analysis of flagellar propulsion," J. Fluid Mech. **184**, 533–549 (1987).
[49] B. Liu, K. S. Breuer, and T. R. Powers, "Propulsion by a helical flagellum in a capillary tube," Phys. Fluids **26**, 011701 (2014).
[50] H. C. Fu, C. W. Wolgemuth, and T. R. Powers, "Swimming speeds of filaments in nonlinearly viscoelastic fluids," Phys. Fluids **21**, 033102 (2009).
[51] S. E. Spagnolie, B. Liu, and T. Powers, "Locomotion of helical bodies in viscoelastic fluids: Enhanced swimming at large helical amplitudes," Phys. Rev. Lett. **111**, 068101 (2013).

[52] J. Blake, "Mucus flows," Math. Biosci. **17**, 301–313 (1973).
[53] S. M. Ross and S. Corrsin, "Results of an analytical model of mucociliary pumping," J. Appl. Physiol. **37**, 333–340 (1974).
[54] G. R. Fulford and J. R. Blake, "Muco-ciliary transport in the lung," J. Theor. Biol. **121**, 381–402 (1986).
[55] M. A. Sleigh, J. R. Blake, and N. Liron, "The propulsion of mucus by cilia," Am. Rev. Respir. Dis. **137**, 726–741 (1988).
[56] D. J. Smith, E. A. Gaffney, and J. R. Blake, "Modelling mucociliary clearance," Respir. Physiol. Neurobiol. **163**, 178–188 (2008).
[57] T. J. Lardner and W. J. Shack, "Cilia transport," Bull. Math. Biophys. **34**, 325–335 (1972).
[58] J. Blake, "Flow in tubules due to ciliary activity," Bull. Math. Biol. **35**, 513–523 (1973).
[59] L. Li and S. E. Spagnolie, "Swimming and pumping of rigid helical bodies in viscous fluids," Phys. Fluids **26**, 041901 (2014).
[60] H. Power and G. Miranda, "Second kind integral equation formulation of Stokes flows past a particle of arbitrary shape," SIAM J. Appl. Math. **47**, 689–698 (1987).
[61] C. Pozrikidis, *Boundary Integral and Singularity Methods for Linearized Viscous Flow* (Cambridge University Press, Cambridge, UK, 1992).
[62] S. Kim and S. J. Karrila, *Microhydrodynamics: Principles and Selected Applications* (Dover Publications, Inc., Mineola, NY, 1991).
[63] K. Atkinson and W. Han, *Theoretical Numerical Analysis* (Springer, New York, NY, 2009).
[64] K. E. Atkinson, *An Introduction to Numerical Analysis* (John Wiley & Sons, New York, 1978).
[65] B. Liu, K. S. Breuer, and T. R. Powers, "Helical swimming in Stokes flow using a novel boundary-element method," Phys. Fluids **25**, 061902 (2013).
[66] M. Sauzade, G. J. Elfring, and E. Lauga, "Taylor's swimming sheet: Analysis and imement of the perturbation series," Phys. D **240**, 1567–1573 (2011).
[67] H. Aref, "Stirring by chaotic advection," J. Fluid Mech. **143**, 1–21 (1984).
[68] R. E. Goldstein, I. Tuval, and J. van de Meent, "Microfluidics of cytoplasmic streaming and its implications for intracellular transport," Proc. Natl. Acad. Sci. U.S.A. **105**, 3663–3667 (2008).
[69] R. B. Bird, R. C. Armstrong, and O. Hassager, *Dynamics of Polymeric Liquids. Vol. 1: Fluid Mechanics* (John Wiley and Sons Inc., New York, NY, 1987).
[70] A. Morozov and S. E. Spagnolie, "Introduction to complex fluids," in *Complex Fluids in Biological Systems* (Springer, 2015), pp. 3–52.
[71] E. Lauga, "Propulsion in a viscoelastic fluid," Phys. Fluids **19**, 083104 (2007).
[72] H. C. Fu, T. R. Powers, and H. C. Wolgemuth, "Theory of swimming filaments in viscoelastic media," Phys. Rev. Lett. **99**, 258101–258105 (2007).
[73] B. Liu, T. R. Powers, and K. S. Breuer, "Force-free swimming of a model helical flagellum in viscoelastic fluids," Proc. Natl. Acad. Sci. U.S.A. **108**, 19516–19520 (2011).
[74] E. Lauga, "Locomotion in complex fluids: Integral theorems," Phys. Fluids **26**, 081902 (2014).
[75] G. J. Elfring, O. S. Pak, and E. Lauga, "Two-dimensional flagellar synchronization in viscoelastic fluids," J. Fluid Mech. **646**, 505 (2010).
[76] T. Honda, K. I. Arai, and K. Ishiyama, "Micro swimming mechanisms propelled by external magnetic fields," IEEE Trans. Magn. **32**, 5085–5087 (1996).
[77] A. Ghosh and P. Fischer, "Controlled propulsion of artificial magnetic nanostructured propellers," Nano Lett. **9**, 2243–2245 (2009).
[78] L. Zhang, J. J. Abbott, L. Dong, K. E. Peyer, B. E. Kratochvil, H. Zhang, C. Bergeles, and B. J. Nelson, "Characterizing the swimming properties of artificial bacterial flagella," Nano Lett. **9**, 3663–3667 (2009).
[79] S. Tottori, L. Zhang, F. Qiu, K. K. Krawczyk, A. Franco-Obregón, and B. J. Nelson, "Magnetic helical micromachines: Fabrication, controlled swimming, and cargo transport," Adv. Mat. **24**, 811–816 (2012).
[80] S. Tottori, L. Zhang, K. E. Peyer, and B. J. Nelson, "Assembly, disassembly, and anomalous propulsion of microscopic helices," Nano Lett. **13**, 4263–4268 (2013).
[81] K. E. Peyer, S. Tottori, F. Qiu, L. Zhang, and B. J. Nelson, "Magnetic helical micromachines," Chem. - Eur. J. **19**, 28–38 (2013).
[82] Y. Tsukii, Protist Information Server, 2005, url: http://protist.i.hosei.ac.jp/.